universität wien

# MASTERARBEIT / MASTER'S THESIS

Titel der Masterarbeit / Title of the Master's Thesis

„Quantifying the uncertainty of empirical models for the icing on structures and wind turbine blades“

verfasst von / submitted by

Clemens Weiß, BSc.

angestrebter akademischer Grad / in partial fulfilment of the requirements for the degree of

Master of Science (MSc.)

Wien, 2018 / Vienna 2018

| | |
|---|---|
| Studienkennzahl lt. Studienblatt / degree programme code as it appears on the student record sheet: | A 066 614 |
| Studienrichtung lt. Studienblatt / degree programme as it appears on the student record sheet: | Meteorologie |
| Betreut von / Supervisor: | Ass.-Prof. Mag. Dr. Manfred Dorninger |

## Abstract

Due to the increasing demand of clean energy, there is an increasing tendency to build wind farms even in locations where severe icing conditions during winter can be detrimental to energy production. This is true also at our latitude, for instance for high-mountain wind farms. Hence, an improvement in the prediction of icing events is necessary. Icing forecasts are typically done by coupling meteorological forecasts and empirical icing models. These models are based on experimentally-derived relationships that estimate the ice mass production from meteorological parameters e.g. liquid water content, droplet concentration, wind speed, temperature and others. The goodness of the icing forecasts depends on the uncertainty of these models. Therefore this thesis focuses on the uncertainties in two empirical icing models, namely the Makkonen model and the iceBlade model.
Icing forecast uncertainty depends both on the imperfect initial conditions, received from a numerical weather prediction (NWP) model and on the inaccuracies in the model. The first component is represented by using an ensemble of different meteorological quantities serving as input parameters to the icing model. These input parameters are obtained by a regional ensemble forecast with the Weather Research and Forecasting (WRF) model. The second component is related to the model uncertainty due to the imperfect representation of the physics inside the icing model. Parameters, connected to this kind of uncertainty are referred to as internal parameters. They are stochastically perturbed between approximately -10% and 10% of their original value inside the model. Finally, case studies are simulated and compared to observations, made at a wind turbine farm in Ellern, Germany during the winter 2016/17.
The uncertainty of ice load forecasts depends mostly on the supercooled liquid water content, the droplet concentration, the wind speed and also most of the time the temperature (input quantities) and on the parameters related to the calculations of the droplet diameter (internal parameter). Both sources of uncertainty can cause a significant ensemble range of the ice load, but due to the dependence of the internal parameters on the input parameters, the input parameters are found to be the key source of uncertainty. Therefore, a future improvement in the generation of the input parameter ensemble as well as in the parametrisations of the meteorological quantities in NWP models, e.g. the liquid water content, is essential.
The Makkonen model predicts the ice load on a small cylindric rod. The iceBlade model is based on the same fundamental equations as the Makkonen model, but it applies them to a simplified wind turbine blade. Throughout the case studies both models are compared with each other, but a general result evaluating the additional value of the expansion of the Makkonen model, cannot be confirmed yet.

## Zusammenfassung

Aufgrund der zunehmenden Nachfrage nach erneuerbarer Energie, steigt die Tendenz, Windparks an Standorten zu bauen, an denen sich Vereisung im Winter negativ auf die Energieproduktion auswirken kann. Dies trifft auch in unseren Breiten zu, z.B. auf Windparks im Hochgebirge. Deswegen ist eine Verbesserung der Vereisungsvorhersage unbedingt notwendig. Für Vereisungsvorhersagen werden typischerweise meteorologische Vorhersagen mit empirischen Vereisungsmodellen gekoppelt. Diese Modelle basieren auf experimentell abgeleiteten Beziehungen, welche die Eisproduktion von meteorologischen Parametern wie z.B. Flüssigwassergehalt, Tröpfchenkonzentration, Windgeschwindigkeit, Temperatur und anderen abschätzen. Die Güte der Vereisungsvorhersagen hängt von der Unsicherheit dieser Modelle ab. Deswegen konzentriert sich diese Arbeit auf die Unsicherheiten zweier empirischer Vereisungsmodelle, nämlich dem Makkonen Modell und dem iceBlade Modell.
Die Unsicherheit der Vereisungsvorhersage hängt sowohl von den fehlerhaften Anfangsbedingungen, erzeugt durch ein numerisches Wettervorhersagemodell und den Ungenauigkeiten innerhalb des Modells ab. Die erste Komponente wird durch ein Ensemble, welches verschiedene meteorologische Größen als Eingangsparameter für das Vereisungsmodell verwendet, repräsentiert. Diese Eingangsparameter werden durch eine regionale Ensemblevorhersage mit dem Weather Research and Forecasting (WRF) Modell gewonnen. Die zweite Komponente hängt mit der Modellunsicherheit, aufgrund der nicht ausreichend berücksichtigten physikalischen Eigenschaften der Vereisungsmodelle, zusammen. Parameter, welche mit dieser Art von Unsicherheit im Zusammenhang stehen, werden interne Parameter genannt. Diese werden im Modell stochastisch zwischen ungefähr -10% und 10% des ursprünglichen Wertes gestört. Zuletzt werden Fallstudien simuliert und mit den Beobachtungen, welche in einem Windpark in Ellern, Deutschland während des Winters 2016/17 gemacht wurden, verglichen.
Die Unsicherheit der Eislastprognose hängt dabei größtenteils vom unterkühlten Flüssigwassergehalt, der Tröpfchenkonzentration, der Windgeschwindigkeit, meistens der Temperatur (Eingangsparameter) und von den Parametern, welche für die Berechnung des Tropfendurchmessers benötigt werden (interne Parameter) ab. Beide Komponenten der Unsicherheit können eine signifikante Ensemblebreite für die Eislast erzeugen, aber aufgrund der Abhängigkeit der internen Parameter von den Eingangsparametern werden letztere als wichtigste Unsicherheit angesehen. Deswegen sind zukünftige Verbesserungen in der Erzeugung des Ensembles sowie in der Parametrisierung meteorologischer Größen in den numerischen Wettervorhersagemodellen, wie dem Flüssigwassergehalt, von enormer Bedeutung.
Das Makkonen Modell sagt die Eislast an einem kleinen zylindrischen Stab vorher. Das iceBlade Modell basiert auf den selben grundlegenden Gleichungen wie das Makkonen Modell, jedoch angewendet auf ein stark vereinfachtes Rotorblatt. Im Zuge der Fallstudien werden beide Modelle miteinander verglichen, ein allgemein gültiges Ergebnis, ob die Erweiterung des Makkonen Modells einen messbaren Mehrwert liefern, kann jedoch nicht ausreichend gegeben werden.

# Acronyms & Abbreviations

| | |
|---|---|
| **CFD** | computational fluid dynamic |
| **ECMWF** | European Centre for Medium - Range Weather Forecasts |
| **GOCART** | Goddard Chemistry Aerosol Radiation and Transport |
| **IEA Wind** | International Energy Agency for wind energy |
| **IMGW** | Institut für Meteorologie und Geophysik |
| **LWC** | liquid water content |
| **MVD** | median volume diameter |
| **NWP** | numerical weather prediction |
| **rpm** | revolutions per minute |
| **SCADA** | Supervisory Control And Data Acquisition |
| **WRF** | Weather Research and Forecasting |
| **WRFMP** | Weather Research and Forecasting multi-physics ensemble |
| **ZAMG** | Zentralanstalt für Meteorologie und Geodynamik |

# Acknowledgement

I would like to thank the members of the ICE CONTROL project for letting me be a part of the project, especially my supervisor Ass.- Prof. Manfred Dorninger for supporting me through the thesis. The ICE CONTROL project was led by the Zentralanstalt für Meteorologie und Geodynamik (ZAMG) and funded by the Österreichischen Forschungsförderungsgesellschaft mbH (FFG).

My special thanks go to Dr. Lukas Strauss and Dr. Stefano Serafin for their tremendous support. They always guided me with a lot of interesting questions and helped me with scientific expertise.

On a personal level, I would like to express my appreciation to my friends and family, especially Sebastian for challenging me through the studies.

# Contents

# 1 Introduction

## 1.1 Motivation

In times of climate change, the usage of renewable energies will become more and more important. World Energy Council (2016) predicts that the world's energy demand will grow intensely, e.g. the demand for electricity will double until 2060. To comply with the set climate targets, based on the Paris Agreement, progress and development in renewable energies such as wind power are needed (United Nations, 2015). As a consequence wind turbine sites also have to be built in cold climate locations. Those regions are defined, according to the International Energy Agency for wind energy (IEA Wind), as areas with frequent atmospheric icing or with periods of temperatures lower than the operational limits of standard wind turbines (Lehtomäki et al., 2016).
Therefore, the wind turbines are exposed to icing, which holds a lot of potential risks. One major problem is the reduction of the wind turbine's lifetime due to icing, since the additional ice mass causes changes in the aerodynamics, which leads to an increase in the component's fatigue loading (WIREs Energy Environ, 2016).
There is also a safety risk for humans and animals provoked by ice throw. Results received within the project „Alpine test Site Gütsch" from 2005 show that ice pieces were thrown up to 92 m far from the turbine, especially during heating of the blades or immediately after the re-start of the turbine after heating. The biggest ice piece found, weighted around 1.8 kg (Laakso et al., 2010).
Nevertheless, one of the major problems is the reduced energy production. Due to icing, the turbine's blade surface roughness changes and increases the drag coefficient, which results in a decrease of the generated wind power. Additionally, there are human-made rules, e.g. mandatory shutdowns at the slightest indication of icing, causing a reduction of the energy production. Figure 1 compares numerically calculated power curves for different icing cases (Turkia et al., 2013).

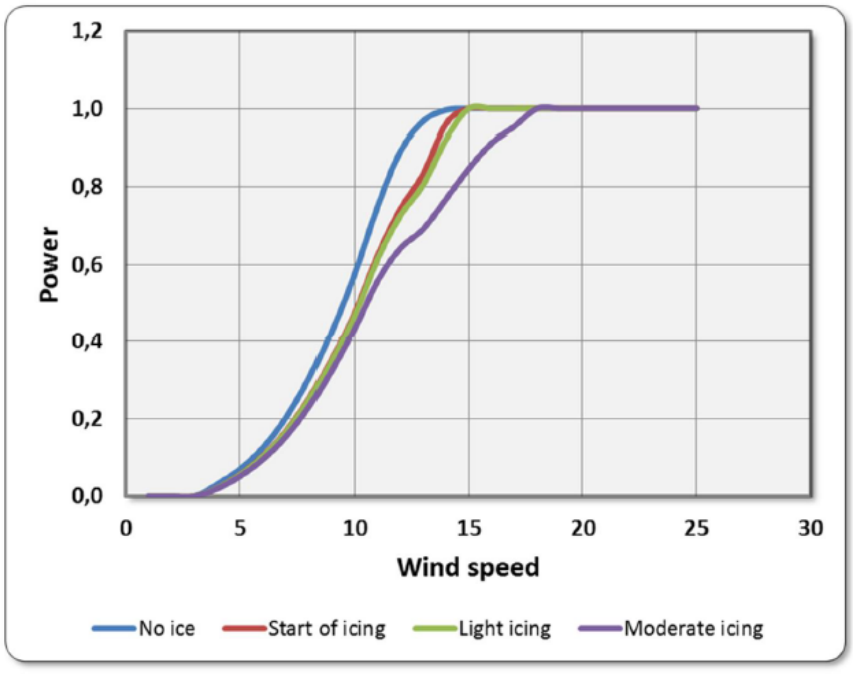


*Figure 1: Normalized power curve simulations for different icing cases. The wind speed is in m $s^{-1}$. The „No ice"-case serves as reference. (Turkia et al., 2013).*

Theoretically the power curve increases from about 3 m $s^{-1}$ (cut-in wind speed) to 25 m $s^{-1}$ (cut-out wind speed) but icing reduces the generated power. If the power is depleted to a certain threshold the wind turbine is shut down and has to be deiced. This is a big problem, because short-term wind power forecasts are used to predict the necessary production of electric energy. By having less power production due to icing, the predicted demand cannot be covered, which results in higher compensation costs. Hence, it is important to be able to predict icing to get an accurate estimate of the produced power (WIREs Energy Environ, 2016).

**Prediction of icing**

This thesis focuses on improving icing models, especially empirical models. Their biggest advantage is that, compared to computational fluid dynamic (CFD) models, empirical models are more cost-efficient and therefore more suitable for forecasts, where the model's running time is of significant importance even though they are not as accurate as the more advanced models (Lehtomäki et al., 2016).
Usually for empirical models there is a common model chain, which is shown in figure 2.

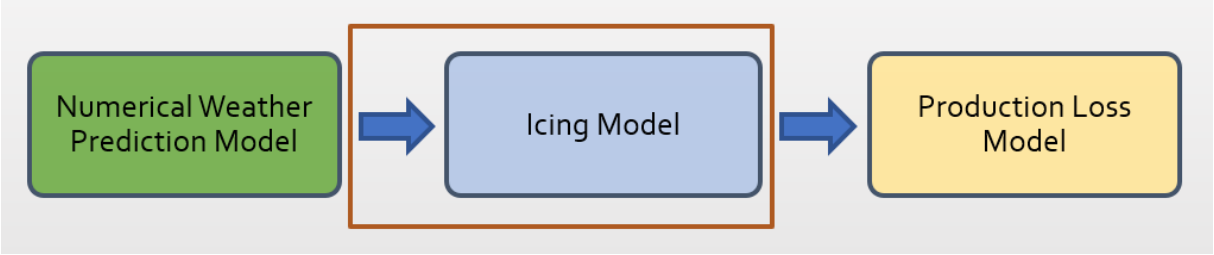


*Figure 2: Common model chain using empirical icing models. The red framed box shows the relevant parts of the model chain, investigated during this thesis.*

First of all there is a numerical weather prediction (NWP) model, which provides the meteorological parameters that are used in the icing model (see section 3.2 for more details). After calculating the ice load via an ice model, a statistical model is used to calculate the icing-related power reduction. Every step of this model chain contains uncertainties, for example the NWP model suffers from the classic issues e.g. imperfect representation of the real topography, insufficient parametrisations of physical processes inside the model, initial conditions and others. Due to the large uncertainties inside the model chain, deterministic forecasts exist, but their skill is only moderate. An ensemble forecast would provide remedy by accounting for the uncertainties. As a consequence, the quality of the icing predictions would be improved. (Davis, 2014; Söderman et al., 2017).

However, the focus of this thesis is put on the uncertainties of the empirical icing models. They will be divided into two categories. The first one includes the errors in the initial conditions, provided by the NWP model. In this thesis, these sources of errors will be specified as uncertainties due to the input parameters. The other category contains the uncertainties, based on the imperfect representation of the physics inside the icing model. This thesis refers to the parameters, related to this type of errors, as internal parameters. As a result, this work tries to answer the following questions:

- To which meteorological quantities (wind speed, temperature,...), serving as input parameters, is the model most sensitive?
- How sensitive is the icing model forecast to variations in the internal parameters?
- Are the uncertainties in the input parameters or in the internal parameters more important?

To answer these questions the Makkonen model and the iceBlade model serve as icing models. They will be introduced in section 2.2. The essential difference between these two models is that the Makkonen model computes icing on a small cylinder, while the iceBlade model applies its computations to a simplified rotor blade. Therefore, additional data, regarding the characteristics of the rotor blade or the status of the turbine, are needed, which will be discussed in section 2.2.2. As a consequence, the necessity of an accurate representation of the rotor blade is investigated as well.

## 1.2 ICE CONTROL

This thesis was carried out within the scope of the ICE CONTROL project, in which representatives of the Zentralanstalt für Meteorologie und Geodynamik (ZAMG) (project management), Institut für Meteorologie und Geophysik (IMGW) from the University of Vienna, the Austrian energy provider VERBUND Hydro Power GmbH and the company Meteotest try to achieve measurable improvements in forecasting icing events. This should be accomplished by using an ensemble prediction system instead of only one deterministic run to predict the final ice load. It is done by taking the many uncertainties inside the model chain into account, which defines the scientific purpose of this work. To quantify the additional value of this approach the following steps will be taken (IMGW, 2017):

- The ensemble predictions will be verified by using wind turbine measurements.
- By using benchmark tests, this attempt will be compared to state-of-the-art icing predictions.
- A cost-loss model will be developed to estimate the value of this approach.
- The prediction model will be tested for different wind turbines in Europe, which are prone to icing.

To compare the icing model predictions, VERBUND provides measurements of meteorological quantities and operational data from a wind turbine sited in a wind farm in Ellern, located on the Hunsrück in the province of Rhineland-Palatinate in Germany, see figure 3. The highest wind turbine is located at 645 m amsl with a hub height of 135 m and a rotor blade length of 63 m. This turbine is also the subject of interest in previous theses, such as Weissinger (2017); Schneider (2017). In-cloud icing, which will be described in section 2.1, is the prevailing cause for icing events in Ellern and therefore icing due to precipitation is of minor importance for this site (Weissinger, 2017). Consequently, the focus in this thesis is mainly on in-cloud icing.

## 1.3 Structure of the work

This thesis consists of seven sections. After a short introduction, section 2 covers the theoretical background of icing models, including a a brief summary about the important types of icing and their formation processes. Additionally, a detailed description of the icing models, in particular the Makkonen

model and the iceBlade model are presented. Section 3 introduces the data used as model input and as observations. The subsection 3.1 contains a short description of the measuring instruments. The sections 4-6 focus on the methodology and the results of this thesis. In section 4 the uncertainties related to the input parameters are discussed, while in section5 the main focus is on the importance of the internal parameters. A comparison between the Makkonen and the iceBlade model is shown in section 6 for real cases. Finally, section 7 summarizes the main findings and lays out future research based on the results of this thesis.


*Figure 3: Map showing the position of the wind farm in Ellern. Taken from Google Earth, Image Landsat/ Copernicus and GeoBasis - DE/ BKG*

# 2 Theoretical Background

## 2.1 Icing on structures

### 2.1.1 Icing processes

According to ISO 12494 (2012), the expression „atmospheric icing “ refers, to all processes, in which water droplets, rain, drizzle or wet snow freeze to any object. Usually atmospheric icing is separated into several formation processes (Andersen et al., 2011):

**Precipitation icing** is icing that arises because of wet snow, freezing rain or freezing drizzle. Freezing rain and freezing drizzle typically go along with an inversion, because for these types to form, a warm air inclusion is needed. Freezing rain occurs, if snow or ice crystals fall into a layer of warm air, melt completely and become rain. As the rain continues to fall, the drops reach a thin layer of cold air below the freezing point but remain in the liquid form as so called supercooled drops. When the drops hit an object, they freeze immediately. Figure 4 shows the typical vertical temperature profile for a freezing rain event (Winter WX, n.d.).

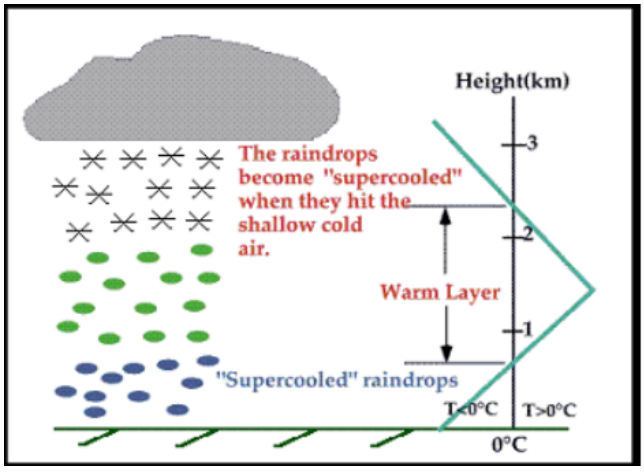


*Figure 4: Vertical temperature profile for freezing rain (Winter WX, n.d.).*

Wet snow usually occurs when the air temperature is just above the freezing point, so when the temperature decreases the free water of the partly melted snow freezes on the object (ISO 12494, 2012). This type of icing especially occurs, if the wind turbine is not in operation. (Ronsten, 2008).

**In-cloud icing** is the other source for icing. It will occur in a saturated environment such as in low clouds or under foggy conditions, where supercooled cloud droplets exist. Typically these droplets hit an object and simply freeze on the surface, if the surface temperature is below 0 °C (Andersen et al., 2011).

### 2.1.2 Ice types

Another way to classify atmospheric icing is to divide it into different types of ice. This is usually done for icing based on supercooled water drops as in in-cloud icing or in icing due to freezing rain and shall be explained briefly in the following paragraphs based on ISO 12494 (2012):

**Rime ice** is the main type of icing regarding in-cloud icing due to the small droplets inside the cloud. Typically it forms on the windward side of the hit object. Due to its windward pointing, vane-like shape, it has a big influence on the aerodynamics of the object. Its density varies between 200 and 900 kg $m^{-3}$ and due to the immediately freezing droplets, often referred to as dry growth, air bubbles cannot escape and as a result rime ice often has a milky colour.

**Glaze ice** is caused by freezing rain or drizzle and also by in-cloud icing, as long as there are very big cloud droplets, resulting in a high supercooled liquid water content (LWC) for each droplet. This type of ice growth is called wet. This means that the droplets do not have enough time to freeze until the next drop hits the surface and as a consequence some drops remain liquid, run off and freeze somewhere else on the object. Due to the long process the air can escape and therefore a transparent and very dense ice is built.

As a first guess it is sufficient to say that bigger drops such as in freezing rain are more likely to create glaze ice and small droplets, which can be found inside of clouds, produce rime ice. On a closer inspection, it is more accurate to also account for temperature, wind speed and the object size. Figure 5 shows the dependence of the ice type on wind speed and on temperature. These curves shift to the left with increasing LWC and to the right with increasing object size.

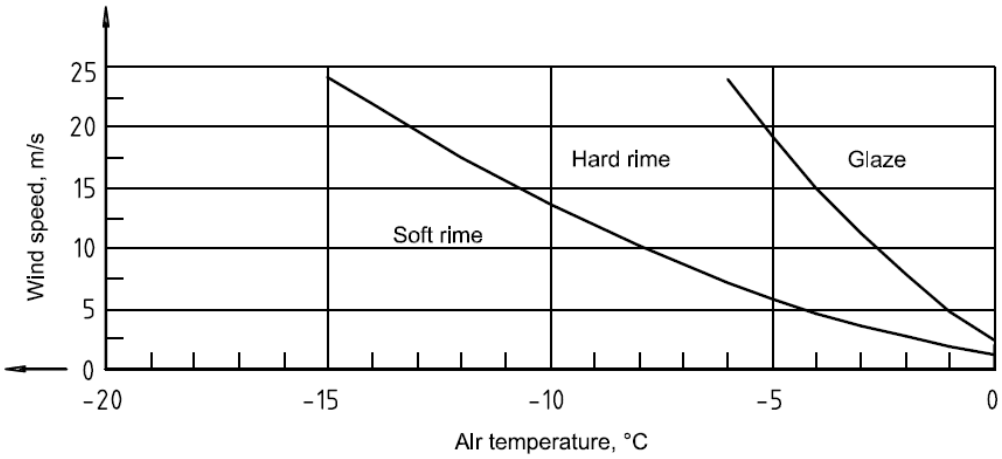


*Figure 5: Icing types dependent on temperature and wind speed. Note that these curves also depend on the LWC and the object size (ISO 12494, 2012).*

Unlike rime ice, glaze ice is less rough and therefore has less impact on the aerodynamics of the object than it is for rime ice. Nevertheless, due to the run off away from the stagnation line, the liquid water freezes somewhere else. Over time, these positions will continue to accrete ice, leading to a formation of horns. They can have a significant effect on the aerodynamics (Homola et al., 2010).

## 2.2 Accretion models

### 2.2.1 Makkonen model

By attempting to use an empirical ice accretion model to predict icing on a structure, many models will rely on the Makkonen Model and also ISO 12494 (2012) refers to this model. Hence, the following section gives an insight into the model's basic principles, based on Makkonen (2000).

This model is based on cloud droplets, raindrops and snow in the air colliding with an object. It is able to predict in-cloud icing and icing due to freezing rain and wet snow. However, due to many uncertainties in the model regarding the prediction of wet snow, only freezing rain and in - cloud icing will be considered in this thesis. This is not a big restriction, because as mentioned in section 1.2,for Ellern icing due to wet snow is not as important as it is due to in-cloud icing.
Usually the Makkonen model uses a reference cylinder rod, which can be seen as a simplified representation of the leading edge of a wind turbine blade. This is a small cylinder with a 0.03 m diameter, rotating around its vertical axis. This design is chosen so that during the ice accretion process the ice load is distributed homogeneously around the cylinder due to a slow rotation. This rotation arises through the imbalance of the cylinder caused by the accreted ice. As a consequence the cylinder will change its diameter but the shape will remain the same during the icing process (Makkonen, 2000).

The maximum ice rate per unit projection area of the object depends on the flux density of the particles hitting the object, which is represented by

$$\frac{\mathrm{d}M}{\mathrm{d}t} = \alpha_1 \alpha_2 \alpha_3 w \boldsymbol{v} \boldsymbol{A} \tag{1}$$

where the icing rate $\frac{\mathrm{d}M}{\mathrm{d}t}$ represents the temporal derivative of the ice load $M$ [kg], which mainly depends on the supercooled liquid water content $w$ [kg m$^{-3}$], on the particle velocity vector $\boldsymbol{v}$ [m s$^{-1}$] and on the the cross - sectional area $\boldsymbol{A}$ [m$^2$] relative to the particle velocity vector. The particle velocity vector is the vectorial sum of the wind- and the droplet fall speed (Makkonen, 2000). As a simplification and also because the fall speed for cloud droplets and the vertical wind speed are very small compared to the horizontal wind speed, the fall speed and the vertical wind speed will be neglected in this work. For rain drops, the fall speed can have an impact on the particle velocity vector, but since in-cloud icing is the prevailing type of icing in Ellern, the fall speed will be neglected as a first approximation. Therefore, $\boldsymbol{v}$ can be simplified to $v$ which represents the absolute value of the horizontal wind speed pointing towards to the object. Furthermore and since the cylinder in this model is not tilted, the cross sectional area in this model can be written as $A$, which is the product of the cylinder diameter and the length of the cylinder. In this thesis, a reference length of 1 m is used for all cylinders. Therefore, the cross sectional area can be replaced by the cylinder diameter $D$ and the unit of the ice load is set to kg m$^{-1}$. So by applying all simplifications to (1), the equation can be rewritten as the following

$$\frac{\mathrm{d}M}{\mathrm{d}t} = \alpha_1 \alpha_2 \alpha_3 w v D. \tag{2}$$

Additionally the ice rate is influenced by the dimensionless $\alpha$-factors, which vary between 0 and 1 and will be introduced below.

**Collision efficiency $\alpha_1$**
The collision efficiency $\alpha_1$ is the ratio of the particles hitting the object to the total amount of particles. Especially small droplets are more likely to follow the streamlines and do not hit the object, as shown in figure 6. This is because for smaller droplets the aerodynamic drag dominates the inertial forces. As a result less LWC is available to freeze on the surface and the icing rate is reduced by this factor (Makkonen, 2000).

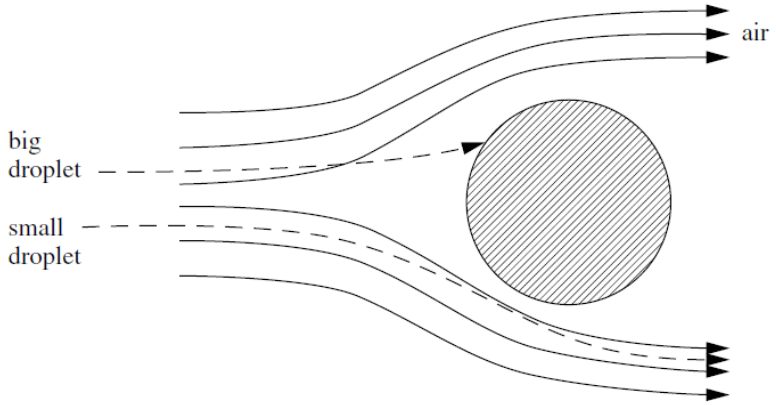


*Figure 6: Theoretical droplet trajectories around a cylinder (Makkonen, 2000).*

Whether a droplet hits the object or gets deflected, depends on the droplet size, the velocity of the air stream and the size of the hit object. This information is used in Finstad et al. (1987), which builds on previous work by Langmuir and Blodgett (1946) to estimate the collision efficiency from numerical simulations for the Makkonen model. In more advanced models the collision efficiency is usually calculated numerically by calculating the droplet trajectories. The major disadvantage is that these calculations need a lot of computation time. Therefore, the Makkonen model uses an empirical fit developed from numerical simulations which is based on two dimensionless parameters $K$ and $\Phi$, where $K$ is the Stokes number and $\Phi$ is the Langmuir Parameter (Finstad et al., 1987) :

$$K = \frac{v\,\rho_w\,d^2}{9\,\mu\,D} \tag{3}$$

$$\Phi = \frac{Re^2}{K} = \frac{9\,D\,\rho_a^2\,v}{\rho_w\,\mu} \tag{4}$$

where the droplet Reynolds number $Re$ is given by

$$Re = \frac{\rho_a\,d\,v}{\mu}. \tag{5}$$

In the equations (3) - (5), $d$ [m] is the droplet diameter, $D$ [m] the cylinder diameter, $\rho_w$ [kg m$^{-3}$] the density of water, $\rho_a$ [kg m$^{-3}$] the density of dry air and $\mu$ [kg m$^{-1}$ s$^{-1}$] the absolute viscosity of air.
In reality, for a given event the droplets will have different diameters. To avoid calculating the collision efficiency for each droplet diameter, the median volume diameter (MVD) [m] is used instead.

It can be shown that using the MVD as a single droplet size approximation is a good approximation regarding the calculations of the collision efficiency (Finstad et al., 1988).
For cloud droplets the MVD can be calculated under the assumption that cloud water follows a generalized gamma distribution. So by calculating the shape parameter $\mu_s$ [1] and the the slope of the distribution $\lambda$ [m$^{-1}$], which mainly depend on the LWC $w$ and on the droplet concentration $Nd$ [m$^{-3}$], one can get the MVD for cloud droplets(Thompson et al., 2009).

$$\mu_s = \min(\frac{10^9}{Nd \cdot 1[\mathrm{m}^3]} + 2,\ 15) \tag{6}$$

$$\lambda = \left(\frac{\pi}{6}\rho_w \frac{\Gamma(4+\mu_s)}{\Gamma(1+\mu_s)} \frac{Nd}{w}\right)^{1/3} \tag{7}$$

Using (6) and (7), the MVD for cloud droplets is calculated by (8).

$$MVD = d = \frac{3.672 + \mu_s}{\lambda}. \tag{8}$$

For rain drops the MVD is set to a constant value of 100 $\mu$m, the lower limit of rain drop diameters (Bergmann and Schaefer, 2001). So in this thesis, the MVD is used synonymously to the droplet diameter.

Using Eq. (8) and calculating $K$ and $\Phi$, the empirical fit to the numerically calculated data can be used to estimate the collision efficiency (Finstad et al., 1987)

$$\alpha_1 = A - 0.028 - C(B - 0.0454) \tag{9}$$

with

$$\begin{aligned} A &= 1.066K^{-0.00616}\exp(-1.103K^{-0.688}) \\ B &= 3.641K^{-0.498}\exp(-1.497K^{-0.694}) \\ C &= 0.00637(\Phi - 100)^{0.381}. \end{aligned} \tag{10}$$

This empirical fit is valid as long as $\Phi$ is between 100 and 10 000 and the Stokes number $K$ is between 0.17 and 1000. The lower limit for $K$ is designed so that the collision efficiency is always positive. It is recommended to use the following values for cases where $K$ is not in the valid range (Finstad et al., 1987).

$$\begin{aligned} \alpha_1 &= 0.01 \quad \text{for} \quad K < 0.17 \\ \alpha_1 &= 0.99 \quad \text{for} \quad K > 10^3 \end{aligned}$$

Except for very small droplets at very low wind speeds the limits of this fit do not cause any major problems for the Makkonen model and also wind tunnel experiments as in Makkonen and Stallabrass (1987) show good agreement between the Langmuir and Blodgett theory and observations for cylinders up to 8 cm. Both Makkonen and Stallabrass (1987) and Finstad et al. (1987) stated that, especially for very small collision efficiencies, the empirical fit becomes more prone to errors due to effects such as air turbulence or surface roughness and therefore shall be treated with caution.

**Sticking efficiency $\alpha_2$**

The sticking efficiency $\alpha_2$ describes the ratio between the droplets sticking on the object to the total amount of the droplets hitting the object. For example for completely solid particles such as dry snow the sticking efficiency tends to zero, because all the particles are likely to bounce off the surface. For water droplets, regardless of cloud or rain droplets, the sticking efficiency can be considered as unity (Makkonen, 2000).

Especially for wet snow, the sticking efficiency is rather important. In literature several attempts to parameterise it, can be found (Makkonen, 2000; Elíasson et al., 2014). Since this thesis focuses on in-cloud icing and slightly on icing due to freezing rain, the sticking efficiency will be used in the following way

$$\alpha_2 \approx 1. \tag{11}$$

**Accretion efficiency $\alpha_3$**

The third quantity with impact on the icing rate is the accretion efficiency $\alpha_3$. This factor determines what portion of the flux density of the particles will be converted to ice. If all of the particles are transformed to ice immediately, the accretion efficiency is not reduced as the process is described as dry growth, which results in the formation of rime ice. For values smaller than unity the latent heat released during the process of freezing can not be removed quick enough so that only a fraction of the droplets freezes and the remaining liquid water runs off. As already mentioned in section 2.1.2 this process is referred to as wet growth, which is typical for the appearance of glaze ice. Figure 7 illustrates schematically the difference between dry and wet growth (Makkonen, 2000).

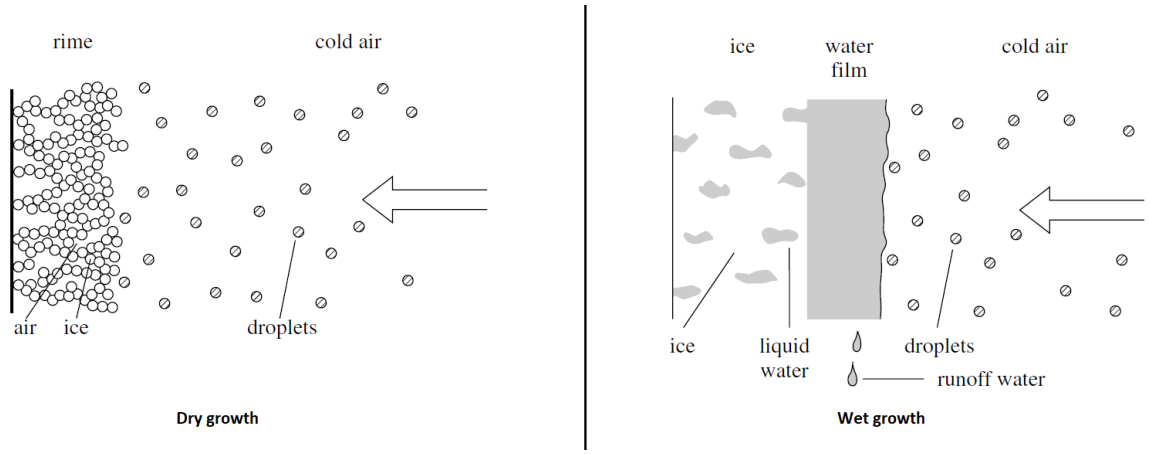


*Figure 7: Schematic presentation of dry growth (left) and wet growth (right) (Makkonen, 2000).*

To estimate the accretion efficiency the Makkonen model uses a heat balance equation for wet growth icing, in which all terms can be parameterised by the meteorological input parameters. In this thesis the heat balance from Makkonen (2000) is used with some minor additions and corrections from Mazin et al. (2001).

$$Q_f + Q_v + Q_a = Q_c + Q_e + Q_l + Q_s \tag{12}$$

Here $Q_f$ [J m$^{-2}$ s$^{-1}$] is the latent heat released during freezing, $Q_v$ [J m$^{-2}$ s$^{-1}$] is the heat flux related to the kinetic energy of the droplets, $Q_a$ [J m$^{-2}$ s$^{-1}$] represents the aerodynamic heating due to compression, $Q_c$ [J m$^{-2}$ s$^{-1}$] parameterises the convective heat transfer, $Q_e$ [J m$^{-2}$ s$^{-1}$] is the heat transfer due to evaporation, $Q_l$ [J m$^{-2}$ s$^{-1}$] represents the warming of the impinging supercooled droplet to the freezing temperature and $Q_s$ [J m$^{-2}$ s$^{-1}$] is the loss of heat due to longwave radiation.
The first assumption is that heat conduction into the ice can be neglected (Makkonen, 2000; Mazin et al., 2001).
Another important assumption is that for wet growth ($\alpha_3 < 1$) the cylinder surface temperature can be assumed to be 0 °C. This is based on the so called „Ludlam limit “, which also describes the process of wet growth. Generally the surface temperature is below zero but it increases due to latent heat released when droplets freeze on the surface. The Ludlam limit is defined as the minimum LWC at which the surface temperature reaches 0 °C. Beyond this limit the temperature will not increase further, instead only a part of the liquid water will freeze immediately on the surface and the rest will run off. (Ludlam, 1951).

The most important term is related to the latent heat which is released during the icing process. It mainly depends on the flux density of the water $F$ [kg m$^{-2}$ s$^{-1}$] hitting the surface because if there is a high flux density, it might happens that only a part of the water can freeze and the rest runs off. Therefore, (13) includes $\alpha_3$ to limit the maximum amount of supercooled water that can freeze on the surface. Additionally some of the water can be entrapped without releasing latent heat. This sponginess correction is depicted by the liquid fraction of the accretion $\lambda$ [1], which is set to 0.3 as a first approximation (Makkonen, 2000).

$$Q_f = (1 - \lambda)\alpha_3 F L_f \tag{13}$$

Here $L_f$ [J kg$^{-1}$] is the specific latent heat of freezing and $F$ can be estimated by

$$F = \alpha_1 \alpha_2 w v \tag{14}$$

The kinetic heat of the droplets is rather insignificant and therefore neglected in Makkonen (2000) but to use the complete heat balance equation this term is parameterised in the following way (Mazin et al., 2001).

$$Q_v = \frac{F v^2}{2} \tag{15}$$

The aerodynamic heating $Q_a$ is also relatively small in the Makkonen model compared to the other heat fluxes. Here, $h$ [J m$^{-2}$ s$^{-1}$ K$^{-1}$] is the convective heat-transfer coefficient, $C_p$ [J kg$^{-1}$ K$^{-1}$] is the specific heat of air and $r$ [1] is the recovery factor for viscous heating, set to 0.79 for a cylinder (Makkonen, 2000).

$$Q_a = \frac{hr\,v^2}{2C_p} \tag{16}$$

Two dimensionless parameters are used to estimate the value of $h$, the Reynolds number for a cylinder $Re_{cyl}$ and the Nusselt number $Nu$ (Makkonen, 1984).

$$Re_{cyl} = \frac{\rho_a\, D\, v}{\mu} \tag{17}$$

$$Nu = 0.032(Re_{cyl})^{0.85} \tag{18}$$

Here (17) is calculated similar to the Reynolds number for droplets in (5), except in (17) the cylinder diameter $D$ is used instead of the droplet diameter. Having the two non-dimensional parameter from (17) and (18), the convective heat-transfer coefficient can be calculated by (Makkonen, 1984).

$$h = \frac{k_a Nu}{D} \tag{19}$$

where $k_a$ [J s$^{-1}$ m$^{-1}$ K$^{-1}$] is the thermal conductivity of air, estimated by (Kochtubajda and Lozowski, 1985).

$$k_a = 2.43 \cdot 10^{-2} + 7.3 \cdot 10^{-4} \cdot T_a[^\circ\mathrm{C}] \tag{20}$$

The convective heat flux $Q_c$ is related to the temperature difference from the surface of the object $T_s$ [K] to the ambient temperature $T_a$ [K]. It can be parameterised the following way.

$$Q_c = h(T_s - T_a) \tag{21}$$

Since $T_a$ has to be smaller than 0 °C to assure that the droplets are supercooled, $Q_c$ is always positive for wet growth conditions and therefore an important term to balance the latent energy term (Makkonen, 2000).
Another important term is the latent heat of evaporation $Q_e$

$$Q_e = \frac{h\,\epsilon\, L_e(E_i - e_a)}{C_p\, p} \tag{22}$$

where $\epsilon$ [1] is the quotient of the specific gas constant of air $R_a$ [J kg$^{-1}$ K$^{-1}$] and the specific gas constant of water vapour $R_w$ [J kg$^{-1}$ K$^{-1}$] ($\epsilon \approx 0.622$), $L_e$ [J kg$^{-1}$] is the latent heat of vapourisation and $p$ [Pa] is the atmospheric air pressure. $e_a$ [Pa] is the vapour pressure in the air. For in-cloud icing it can be assumed that the air is saturated with respect to water and therefore in most of the icing cases $e_a$ only depends on the temperature. $E_i$ [Pa] is set to 6.11 hPa by using the Goff-Gratch equation to determine the saturation vapour pressure over ice in respect to the surface temperature of 0 °C (Mazin et al., 2001).

The term $Q_l$ is based on the difference between the temperature of the impinging droplets and the surface temperature. Especially for cloud droplets, due to theirs small fall speed, it can be assumed that the droplets have the same temperature as their environment. Therefore, $Q_l$ can be written as

$$Q_l = F\, C_w (T_s - T_a) \tag{23}$$

where $C_w$ [J kg$^{-1}$ K$^{-1}$] refers to the specific heat of water (Makkonen, 2000).

The last term $Q_s$ is related to the influence of the radiation. Since icing occurs under cloudy and foggy conditions the short wave radiation is neglected and the heat loss only happens due to longwave radiation. Assuming emissivities of unity, $Q_s$ can be parameterised as

$$Q_s = \sigma a (T_s - T_a). \tag{24}$$

Here, $\sigma$ is the Stefan-Boltzmann constant ($5.67 \cdot 10^{-8}$ J s$^{-1}$ m$^{-2}$ K$^{-4}$) and $a$ refers to the radiation linearisation constant ($8.1 \cdot 10^{7}$ K$^3$) (Makkonen, 2000).

By using the parametrisations of the heat fluxes in (12) and isolating $\alpha_3$ on one side, the accretion efficiency can be calculated by

$$\alpha_3 = \frac{1}{(1-\lambda) F\, L_f} \left[ (h + \sigma a)(T_s - T_a) - h \frac{r v^2}{C_p} - \frac{F v^2}{2} + \frac{h\, \epsilon\, L_e (E_i - e_a)}{C_p\, p} + F C_w (T_s - T_a) \right]. \tag{25}$$

After calculating the three efficiencies, it is possible to calculate the ice rate for one time step by using (2), to get the ice load. Since icing is a time-dependent process, numerical methods are needed. The most fundamental change during an icing event is the modification of the cylinder diameter. In the beginning of this section a simplification was made, assuming that the cylinder accretes the ice homogeneously on his surface and therefore his cylindrical shape remains continuously. As a consequence the cylinder diameter has to increase due to the accumulation of ice. As a consequence, this affects the calculations of the collision and accretion efficiency and the ice rate in the next time step. It is therefore important to calculate the density of the ice and, by using the geometric properties of the cylinder, to adjust the cylinder diameter (Makkonen, 2000).

In this thesis the ice density $\rho$ [kg m$^{-3}$] is estimated by an empirical fit based on wind-tunnel experiments (Makkonen (2000) cited from Makkonen and Stallabrass (1984))

$$\rho = [0.378 + 0.425(\log R) - 0.0823(\log R)^2] \cdot 1[\mathrm{kg\,m^{-3}}] \tag{26}$$

where $R$ [1] is the Macklin's parameter (Macklin, 1962).

$$R = -\frac{v_0\, d[\mu m]}{2\, T_a[^\circ\mathrm{C}]} \cdot 1[^\circ\mathrm{C\,m^{-2}\,s}] \tag{27}$$

In Macklin (1962) the surface temperature $T_s$ is used instead of temperature of the air $T_a$ but because usually the release of latent is too small to heat the surface significantly, $T_s$ can be approximated by $T_a$ (Makkonen, 2000). $v_0$ [m s$^{-1}$] is the droplet impact speed and can be calculated the following way (Makkonen, 1984).

$$K_0 = K(0.087 Re^{0.76 Re^{-0.027}} + 1)^{-1} \tag{28}$$

where $K$ and $Re$ are the same dimensionless parameters received from (3) and (5). Using $K_0$ [1] one can get $v_0$ by

$$\begin{aligned} v_0 &= v(-0.174 + 1.464 K_0 - 0.816 K_0^2) \qquad \text{for} \quad K_0 \leq 0.55 \\ v_0 &= v\{0.561 + 0.592 \log(K_0) - 0.26[\log(K_0)]^2\} \qquad \text{for} \quad K_0 > 0.55. \end{aligned} \tag{29}$$

The empirical fit in (26) is primarily made for rime icing, but as a simplification this fit is used for all icing cases. After calculating the density for the ice caused by cloud droplets and by freezing rain, the cylinder diameter can be updated using simple geometric relations. Being able to adjust the cylinder diameter every time step makes it possible to simulate time-dependent icing on a cylinder and allows to accumulate the ice load over a certain time span. Figure 8 schematically shows the model cycle for each time step.

### 2.2.2 iceBlade model

The iceBlade model is an extension of the Makkonen model, which basically uses the same equations as the Makkonen model introduced in the previous subsection. It is applicable to model icing due to supercooled liquid water, namely in-cloud icing and icing due to freezing rain. Some upgrades and simplifications are made to expand the ability to predict icing from a small cylinder to a simplified wind turbine blade. Additionally the iceBlade model contains terms for sublimation, ice shedding and wind erosion, which will not be explained here in detail. The key concepts of the updated ice accretion process are introduced in the following, based on Davis (2014):

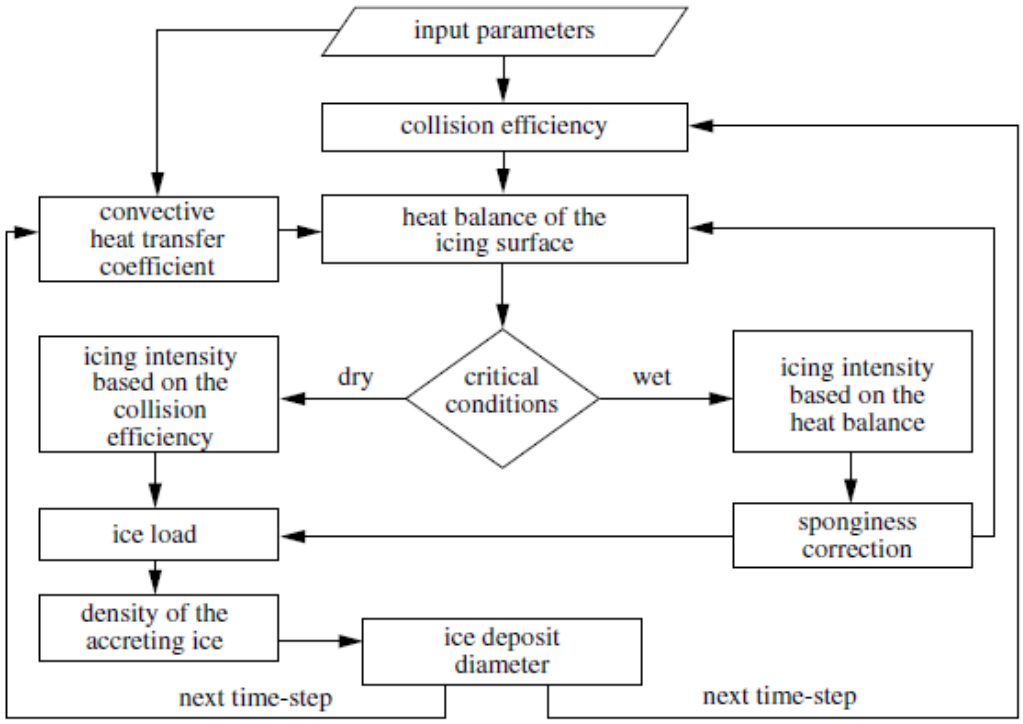


*Figure 8: Block - diagram showing the model cycle (Makkonen, 2000).*

**Simplifications related to the input parameters**

Just like the Makkonen model, the iceBlade model uses input parameters provided by a NWP model. As a simplification, only the input parameters at the hub height are used, independent from the selected position on the blade. This is done in order to avoid the need to know the exact position of the blade during one revolution (Davis, 2014).

**Blade-relative velocity**

One quite significant difference is the increase of the free stream velocity. In the Makkonen model this velocity is synonymous to the wind speed but in the iceBlade model the rotation of the wind turbine blade is also taken into account. Therefore, the wind speed $v$ is changed to the blade-relative velocity $v_b$ [m s$^{-1}$]. The blade-relative velocity mainly depends on the geometry, especially on the length of the blade, so for positions closer to the tip the additional contribution to the velocity by the rotation of the blade is larger than for positions closer to the hub (Davis, 2014).

An empirical fit is used to estimate the revolutions per minute (rpm) from the ambient wind speed, based on wind turbine data. After computing the angular velocity $\omega$ [rad s$^{-1}$] in SI units

$$\omega = \frac{2\pi}{60}\, rpm \tag{30}$$

the tangential velocity $v_t$ [m s$^{-1}$] at a given position can be calculated by

$$v_t = r\,\omega \tag{31}$$

where $r$ is the distance between the selected position and the hub. If the ambient wind speed is smaller than the cut-in wind speed, the wind turbine has a standstill and therefore the tangential velocity is zero. Finally the blade-relative velocity $v_b$ can be calculated by (32) (Davis, 2014).

$$v_b = \sqrt{v^2 + v_t^2} \tag{32}$$

**Turbine blade representation**

Another crucial factor is the representation of the wind turbine blade. In the original version of the iceBlade model from Davis (2014), a 1 m long blade segment is taken, located at about 85% of the blade's length away from the hub. The blade is approximated by a cylinder of the length 1 m, shown in figure 9. While the Makkonen model has been tested with cylinder diameters up to approximately 8 cm (Makkonen and Stallabrass, 1987), the cylinder diameters in the iceBlade model are generally bigger, because the leading edge curvature radius of the wind blade is larger. The exact diameter is also dependent on the turbine type and the position on the blade. Based on the blade of a reference turbine cited in Jonkman et al. (2009), the blade segment located at 85% of the blade's length has a cylinder diameter of about 0.144 m (Davis, 2014).

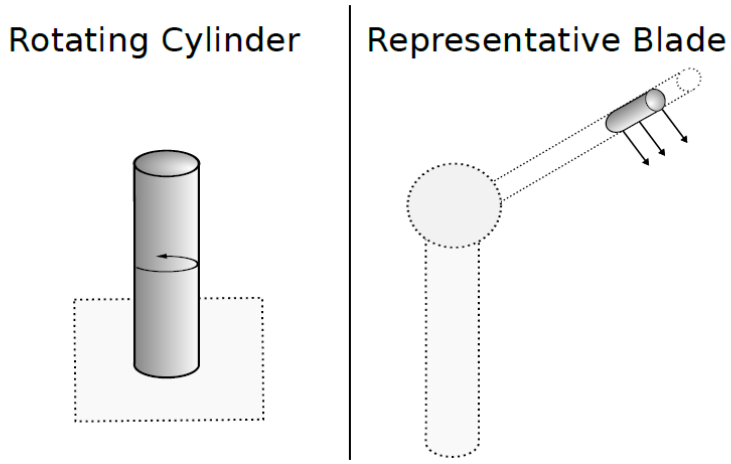


*Figure 9: Comparison between the object representation in the Makkonen model (left) and the iceBlade model (right) (Davis, 2014).*

**Cylinder diameter update**

The Makkonen model assumes that the ice accretes homogeneously around the cylinder in order to keep its shape. In the iceBlade model another approach is taken. Simulations using CFD models showed that for an airfoil most of the ice forms on the leading edge of the blade (Homola et al., 2010). Therefore, the iceBlade model assumes that ice accretion does not increase the size of the surface where icing occurs (Davis, 2014). As a consequence the terms in the Makkonen model related to the update of the cylinder diameter (26) - (29), are omitted in the iceBlade model.

# 3 Data

## 3.1 Observations

In order to verify the results established by the icing models and to compare the model's input parameters with the reality, the ICE CONTROL Project is able to access to operational measurement data. These measurements are provided by a wind turbine in a wind farm in Ellern, as mentioned in 1.2. In the course of the ICE CONTROL project additional instruments were deployed, tailored to the parameters of interest concerning ice detection. Table 1 gives an overview of the measurement instruments available for the winter 2016/17 and the parameters, which are used in this thesis. The icing related parameters such as the ice load or the icing rate from the devices at the nacelle are used to verify the predictions made by the Makkonen model, while the eologix sensor measurements, introduced in this section later, are compared with the iceBlade predictions. As in the model, explained in section 2.2.2, the meteorological input parameters do not differ regarding their spatial distribution. Therefore, the meteorological parameters i.e. temperature, wind speed, humidity and others, measured at the nacelle are used to validate the Makkonen model as well as the iceBlade model.

| | Measured Parameters | Application |
|---|---|---|
| Rotronic sensor | T, RH | nacelle |
| IceMonitor | ice load | nacelle |
| Camera Images | ice load, ice rate | nacelle |
| Operational wind turbine data | ff, power, rpm, T, icing (1/0), heating (1/0) | nacelle/blade |
| eologix | ice signal, $T_s$ | blade |

*Table 1: Overview of the measurement instruments used at the wind turbine in Ellern*

Hereinafter, a short description of the instruments is given:

**Rotronic sensor**
The Rotronic sensor measures the temperature (T) and the relative humidity (RH) [%] and is protected by a radiation shield. This shield causes problems under icing conditions. During an icing event the cover can freeze completely on the outside and as a result the relative humidity sensor registers around 100 % relative humidity continuously. This ice layer acts as a dividing wall between the sensors and the ambient air. Therefore, the temperature measured during icing event, only represents the temperature inside the ice layer. Nonetheless, the Rotronic sensor seems to be the most representative instrument measuring temperature and will be used to verify the modelled temperatures. Due to the special behaviour of the relative humidity sensor during icing conditions, the relative humidity measured on the nacelle, see figure 10, can be used to estimate the beginning and ending of meteorological icing periods on the nacelle. Consistent with the assumption in section 2.2.2, the temperature measured by the Rotronic sensor is also used to represent the ambient air temperature around the turbine blades (Schneider, 2017).

**IceMonitor**
The IceMonitor is the equivalent to the cylinder in the Makkonen model, described in section 2.2.1. It is an instrument, represented by a cylinder with a diameter of 30 mm, slowly rotating around its vertical axis. The cylinder length, as long as the ice accretion is not expected to be heavy, is 0.5 m (ISO 12494, 2012). The IceMonitor placed on the nacelle, as shown in figure 10, measures the ice load by a

load cell. The accreted ice on the cylinder leads to an asymmetrical shape and therefore the cylinder starts to rotate around its vertical axis. In order to minimize friction and to avoid icing on the base an electrical heating system is used (Cattin and Heikkilä, 2016).

Although the IceMonitor seems to be the best instrument to compare the results of the Makkonen model, Schneider (2017) shows some major shortcomings of the measurement cylinder, which are also noticed in other research projects.

One big problem is that even though heating should prevent the cylinder to freeze onto the base, there are situations, when the rod freezes in anyway. Therefore, the ice load can not be measured anymore and sometimes there are even negative ice load values caused by the ice lifting the cylinder (Cattin and Heikkilä, 2016).

Another issue is that the IceMonitor was originally designed to measure icing on power lines and high ice loads (Cattin and Heikkilä, 2016). As a consequence, the instrument can not cope with light ice accretion and there are many cases where the camera images, explained next, showed icing while the IceMonitor reported nothing at all (Schneider, 2017).

Other issues such as vibrations causing noisy outputs or uneven ice accretion on the cylinder can be found in detail in Schneider (2017). Based on the many shortcoming, the IceMonitor is only used to approximately estimate the ice load at the nacelle.


*Figure 10: Camera images for the 31.12.2016 09:40 UTC (left) and the 04.01.2017 13:40 UTC (right), directing to the nacelle. Made by Meteotest.*

**Camera Images**

In the course of the project three cameras were installed on the turbine hub. One is oriented towards the sensors on the nacelle, including the Rotronic sensors and the IceMonitor, the other two cameras show images of the rotor blade. Meteotest, one of the project partners mentioned in section 1.2,

classified the images based on the camera directed to the nacelle, as shown in figure 10. Therefore the icing rate and the ice load are categorised by:

- icing rate: light, moderate and strong
- ice load: light, light - moderate, moderate, moderate - heavy and heavy

Especially during day time the camera images are a reliable source for icing on the nacelle and it is also possible to distinguish between in-cloud icing and icing due to precipitation. During the night it is harder for an observer to notice surrounding clouds (Schneider, 2017). The greatest source of error is the observer, because there is always a subjective evaluation, which might be different, dependent on the observer. Nevertheless it is assumed that the camera images provide the best results concerning ice detection on the nacelle. Figure 11 shows the results of the camera image classification for the winter 2016/17. It can be seen that in this winter for the wind turbine in Ellern the frequency of significant icing events was rather small.

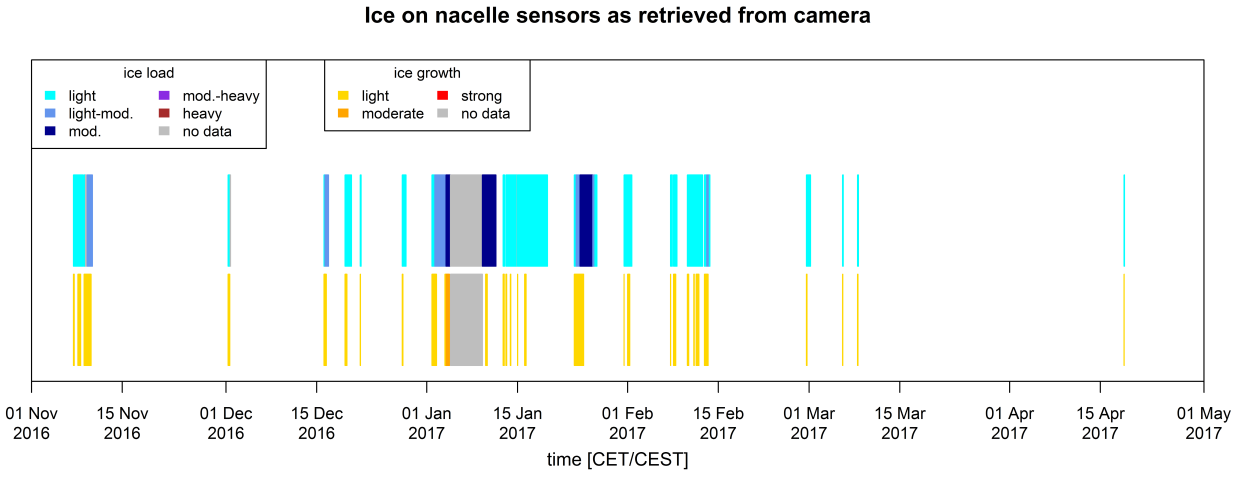


*Figure 11: Camera image classification for the winter 2016/17 for a wind turbine in Ellern, made by Meteotest.*

**Operational wind turbine data (SCADA)**

Supervisory Control And Data Acquisition (SCADA) is a system used in industries e.g. energy, recycling, transportation and many more to promote efficiency and exploit data for an improved decision making by using a combination of software and hardware elements (Krambeck, 2015).
For the wind farm in Ellern a SCADA system is used to monitor the turbine performance. The monitoring of icing is an integral part of this system. The data necessary to run it are temperature (T), wind speed (ff), wind direction (dd) [°], revolutions per minute (rpm) and produced power [J $s^{-1}$]. For the wind data there is also a quality control flag, because the correctness of the wind data is only ensured for a rotating wind turbine. The power curve, as in figure 1, serves as indicator for icing on the rotor blades. If the power production is significantly smaller than the expected power according to the mean power curve of the turbine, the wind turbine is shut down due to icing and the turbine's supervisor has to turn on the blade heating. A binary time series is made for the signals of icing and blade heating (Schneider, 2017).

**eologix sensors**
The eologix sensors are able to detect icing on the wind turbine blade. Therefore, 26 sensors are distributed over three rotor blades and two sensors are installed on the nacelle (Burchhart, 2017).
The measurement is based on the influence of the accreted ice on the impedance of the eologix sensor. Each sensor measures a temperature and gives an ice signal related to the estimated ice thickness (VERBUND, 2016; Cattin and Heikkilä, 2016):

- ice signal = 1: free surface
- ice signal = 2: wet or ice thickness < 1 $mm$
- ice signal = 3: ice thickness > 1-2 $mm$
- ice signal = 4: ice thickness > 10 $mm$

Here the ice signal depends also on the ice type, so there is a difference between rime ice and glaze ice, which one has to be aware of looking at the ice signal data (Burchhart, 2018). The measured temperatures depend strongly on external influences such as for example on the blade heating or on radiation. Therefore, the eologix temperatures are understood as blade surface temperatures instead of representing the ambient air.
In this thesis not all sensors are used, only these listed in table 2, located on the leading edge of the blade. Figure 12 shows one eologix sensor installed on the leading edge.

| Sen. | 821 | 915 | 897 | 877 | 888 | 839 | 898 | 912 | 887 | 896 | 914 | 1007 | 852 | 864 | 1006 |
|---|---|---|---|---|---|---|---|---|---|---|---|---|---|---|---|
| Dist. | 6 | 6 | 16 | 26 | 26 | 36 | 46 | 46 | 58 | 58 | 58 | 60 | 62 | 62 | 62 |

*Table 2: List of all used eologix sensors on the leading edge of the rotor blade and their distance to the root [m] for a wind turbine in Ellern.*

## 3.2 Model input data

As mentioned in section 1.1, the ice model receives its input parameters from a NWP model. For the Makkonen model as well as for the iceBlade model the necessary input parameters are:

- Temperature $T$ [K]
- Wind speed $v$ [ms$^{-1}$]
- LWC for cloud droplets $w$ [kg m$^{-3}$]
- Cloud droplet concentration $Nd$ [m$^{-3}$]
- LWC for rain drops $wr$ [kg m$^{-3}$]
- Pressure $p$ [Pa]
- Specific humidity $q$ [kg kg$^{-1}$]

For tests regarding the general behaviour of the model under specific circumstances synthetic data are used, which will be described in more detail in section 4.


*Figure 12: eologix sensor on the leading edge of the rotor blade (Burchhart, 2017).*

To run the ice model under real conditions during the winter 2016/17, an ensemble of Weather Research and Forecasting (WRF) model simulations are used, provided by members of the ICE CONTROL project, to receive the necessary input parameters. The simulations are run for two different domains, as shown in figure 13, where the bigger region D01 has an horizontal resolution of 12.5 km and the nested domain D02 has a horizontal grid spacing of 2.5 km. In the vertical the WRF model uses 51 levels and the initial conditions are taken from European Centre for Medium - Range Weather Forecasts (ECMWF) ensemble prediction system members. The model is initialised at 00 UTC for every day and the prediction period is up to 60 h. To reduce errors caused by the imperfect model topography, certain points are enhanced and adjusted to the real topography under consideration of the possible gradients of the terrain. The real topography is 645 m amsl at the wind turbine in Ellern, while the adapted height inside the model is 514 m amsl for D01 and 590 m amsl for D02.

As mentioned in section 1.1, one source of error in the empirical icing models is related to the uncertainties in the input parameters, received from a NWP model. To cope with these uncertainties an ensemble, having different initial conditions each run, is used. Different ways of generating an ensemble were tested, for example using one WRF setup coupled with 10 representative ECMWF ensemble members, but the biggest spread and the best performance was found to be achieved by using a Weather Research and Forecasting multi-physics ensemble (WRFMP). Different combinations of meteorological parametrisations for the boundary layer, the microphysics and others are used, listed in table 3. Finally, there is one control run (WRFCT) and 10 members of the WRFMP, representing the uncertainties due to the errors in the initial conditions of the icing models.

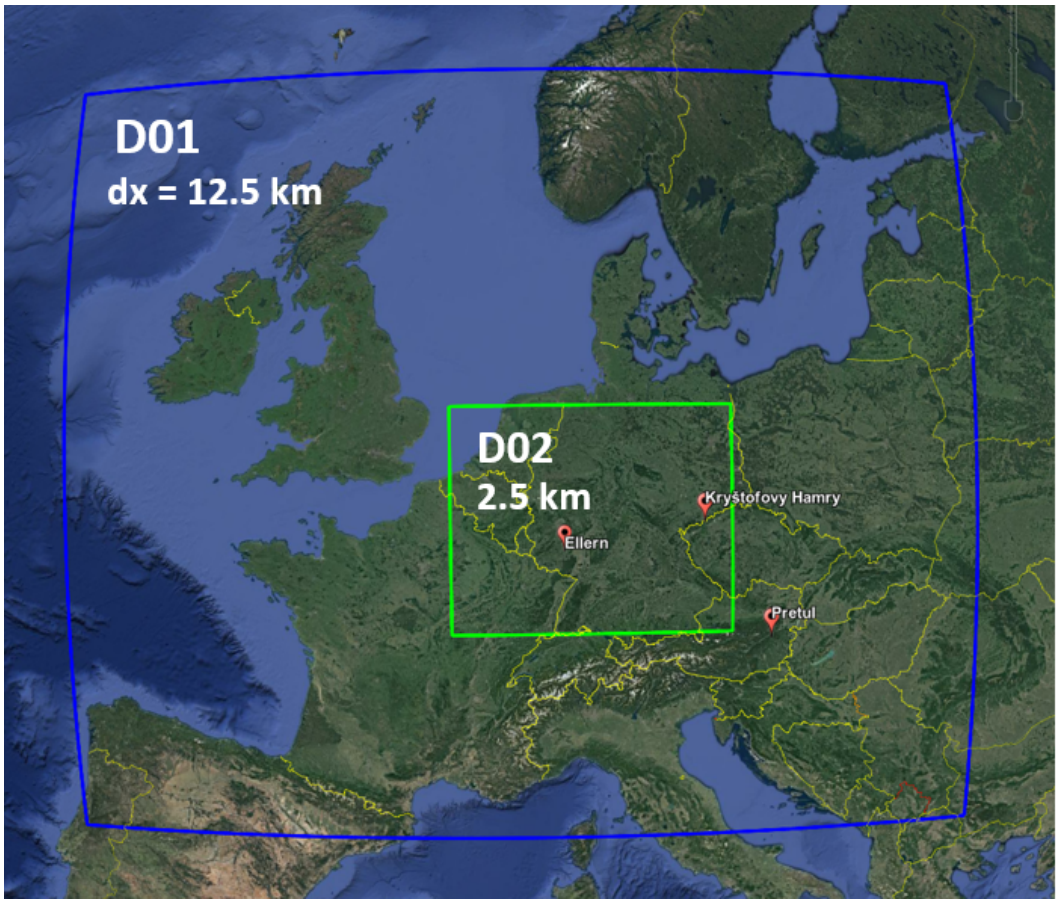


*Figure 13: WRF domains used to generate the input parameters for the ice model. Beside Ellern, two additional wind farms are charted, which are probaly used in the future within the project (Strauss and Serafin, 2018).*

| | BOUNDARY LAYER | SURFACE LAYER | MICRO-PHYSICS | LAND-SURFACE MODEL | LAND-USE DATA | Δ w.r.t WRFCT |
|---|---|---|---|---|---|---|
| WRFCT | MYNN | MYNN | T&E AE | RUC | MODIS | 0 |
| WRFMP M01 | BouLac | MOJ | Thompson | RUC | CORINE | 3 |
| WRFMP M02 | YSU | Revised MO | Morrison | NOAH | MODIS | 3 |
| WRFMP M03 | MYNN | MYNN | Morrison | NOAH | CORINE | 3 |
| WRFMP M04 | YSU | Revised MO | Thompson | RUC | MODIS | 2 |
| WRFMP M05 | YSU | Revised | T&E AE | NOAH | MODIS | 2 |
| WRFMP M06 | BouLac | MOJ | Morrison | NOAH | MODIS | 3 |
| WRFMP M07 | QNSE | QNSE | Thompson | NOAH | MODIS | 2 |
| WRFMP M08 | MYNN | MYNN | Thompson | RUC | CORINE | 2 |
| WRFMP M09 | BouLac | MOJ | T&E AE | NOAH | CORINE | 3 |
| WRFMP M10 | QNSE | QNSE | Thompson | NOAH | CORINE | 3 |
| # schemes | 4 | 4 | 3 | 2 | 2 | |

*Table 3: WRFMP used to cover the uncertainties in the icing model input parameters. WRFCT represents the control run, while the other members use different boundary-layer and microphysic schemes in the WRF model (Strauss and Serafin, 2018).*

# 4 Sensitivity of icing predictions to boundary conditions

## 4.1 Methodology

To answer the question of to which meteorological parameters the model is most sensitive and to understand, how the input parameters affect the resulting ice load, different scenarios are simulated. Since, according to Weissinger (2017), the prevailing mechanism for icing in Ellern is in-cloud icing, the focus is on the meteorological parameters necessary to model it, namely temperature $T$, wind speed $v$, LWC of cloud droplets $w$ and droplet concentration $Nd$. The pressure and the specific humidity are input parameters as well, but due to their secondary role, explained in this section, the pressure will be set to 1000 hPa and the specific humidity will be selected in a way that the relative humidity is at 100% during the icing events. Simulations aim at quantifying how much the ice load forecasts depend on small variations in the input parameters. For every simulation one parameter is varied, while the other parameters are set constant, hence it is possible to estimate the impact of every single parameter. It should be noted that this is only a cross-section through the phase space of the possible input parameters and using different constants might lead to different results. To achieve the most general results, the constant parameters are selected in a way that they represent a characteristic value of their natural range. Table 4 shows the selection of the constant parameters, as well as the interval, in which each parameter is varied. All these tests are applied to the typical Makkonen cylinder, having a cylinder diameter of 0.03 m.

| | Constant values | Range of the variations |
|---|---|---|
| Temperature $T$ [°C] | -3 | [-5; 1] |
| Wind speed $v$ [m s$^{-1}$] | 12 | [0; 20] |
| LWC of cloud droplets $w$ [g m$^{-3}$] | 0.8 | [0.2; 1.0] |
| Droplet concentration $Nd$ [cm$^{-3}$] | 300 | [100; 500] |

*Table 4: Synthetic input parameter*

## 4.2 Results and Discussion

To understand the sensitivity of the model to the input parameters, it is necessary to know where they have the biggest impact inside the model. The following subsection investigates the influence of each input parameter in the Makkonen model and based on the parameter's impact, as well as the availability of measurements to justify the results, the model's sensitivity is estimated.

**LWC**

One of the most important parameters is the liquid water content. It is the amount of supercooled liquid water, which can freeze on the object. Figure 14 shows the effect for different LWC values on the ice load, where the yellow line represents a high amount of liquid water, while the black line shows the minimum, see figure 14 b). To improve clarity a step function is used for the LWC. Together with the droplet concentration, the liquid water content is needed to calculate the MVD, which represents the droplet size, i.e. for a higher liquid water content the drops become bigger. Eq. (3) reveals that bigger drops lead to bigger Stokes numbers and as a consequence to that, to a higher collision efficiency $\alpha_1$. This makes sense, because as explained in section 2.2.1 bigger droplets are more likely to hit the object than smaller ones due to their higher inertia. Finally, a higher supercooled LWC results in a higher icing rate due to the increased collision efficiency and also due to the direct effect of

the LWC in the basic equation (2). Though, with increasing ice load the cylinder diameter becomes bigger, which on one side increases the icing rate directly in (2), on the other side a bigger cylinder diameter reduces the Stokes number and therefore the collision efficiency. This explains the decline of the collision efficiency in figure 14. The effect of the increasing cylinder diameter can also be seen in the ice rate. With an increasing diameter, the icing rate reaches its maximum but after a while the decrease in the collision efficiency compensates this effect and the ice rate decreases.

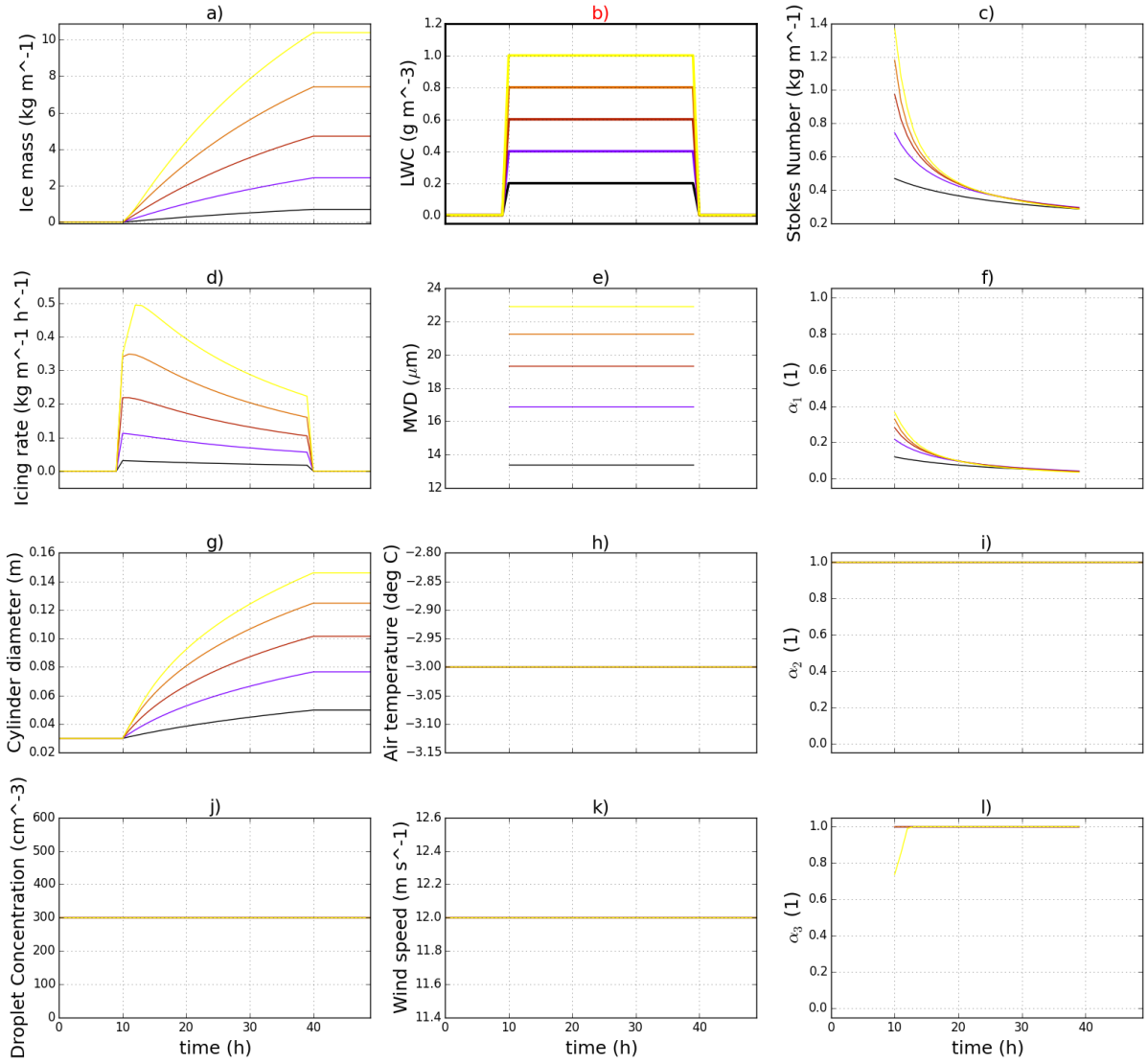


*Figure 14: The behaviour of the Makkonen model for different liquid water contents at constant droplet concentrations as input parameters.*

The LWC does not only effect the collision efficiency, but also the accretion efficiency $\alpha_3$. Especially for very large drops with high LWC, the released latent heat due to the freezing process is rather big and therefore, some of the supercooled water remains liquid and runs off. This does not only depend on the LWC but also on the other input parameters as well as on the collision efficiency, since the collision efficiency determines, how much supercooled water hits the object. In figure 14 one can see that the yellow line, which represents the highest LWC case, starts with an accretion efficiency

smaller than unity but as the collision efficiency decreases, the accretion efficiency increases due to the smaller amount of supercooled liquid water.
In the WRF model, the LWC is calculated by using microphysical schemes. Under real circumstances, it is hard to measure the LWC and there are several attempts to find ways to estimate the LWC from other meteorological parameters such as visibility or cloud height (Pedersen et al., 2018).
Since the LWC has a key role in each of the basic equations and due to the difficult accessibility, the LWC is one of the most important parameters in the model.

**Droplet Concentration**

The droplet concentration is strongly related to the LWC. Figure 15 shows the impact of a different number of droplets within a specific volume. The yellow line in figure 15 j) represents a high concentration of 500 droplets within one cubic centimeter, while the black line means that there are only 100 droplets within one cubic centimeter. Since the LWC is the same for all scenarios, the droplets considered for plotting the yellow have to be much smaller than the drops for the black line, because for each droplet there is less water available if there are many droplets. Contrary to the LWC, the droplet concentration does not have a direct influence on Eq. (2), but together with the LWC, it is an essential parameter regarding the droplet size. Therefore there are the same indirect effects as for the LWC, which will not be explained again.

Similar to the LWC, the droplet concentration in the WRF model is also calculated by using a microphysical scheme. There are two different approaches regarding the droplet concentration. There are schemes, which use a constant droplet concentration over the whole period and there are schemes which have internal equations calculating the droplet concentration. It was found that for aircraft icing an accurate prediction of the droplet concentration is rather important (Thompson et al., 2017). The droplet concentration depends on the concentration of cloud condensation nuclei, which are related to some kinds of aerosols. Nevertheless, the uncertainties regarding e.g. the prediction of the aerosols needed in this model, are rather big. Thompson and Eidhammer (2014), for example, uses the aerosol concentration derived from global simulations by the Goddard Chemistry Aerosol Radiation and Transport (GOCART) model and interpolates them to the horizontal and vertical points to use them as initial and boundary conditions.

The impact of the droplet concentration is comparable to the LWC's impact and due to the great uncertainties in modelling and measuring it, the droplet concentration is as important as the LWC.

**Wind speed**

Another important input parameter is the wind speed. Since we are describing the Makkonen model for the moment, there is no additional term related to the rotation of the blade and because the droplets terminal speed is neglected, the velocity $v$ in the equations of section 2.2.1 is only the wind speed. Figure 16 shows the model's behaviour for different wind speeds, where the yellow line is the largest (20 $m/s$) and the black line represents the smallest wind speed (0 $m/s$). The biggest difference of figure 16 compared to the previous figures is that changes in the wind speed do not have any influence on the droplet diameter. But the impact on the final ice load is similar compared to the effects provided by the LWC and the droplet concentration. The wind speed has a direct influence on the resulting ice rate, which can be seen in (2). By looking into (3), one can easily see that the Stokes number increases with increasing wind speed and as a result the drops are more likely to hit the object, which

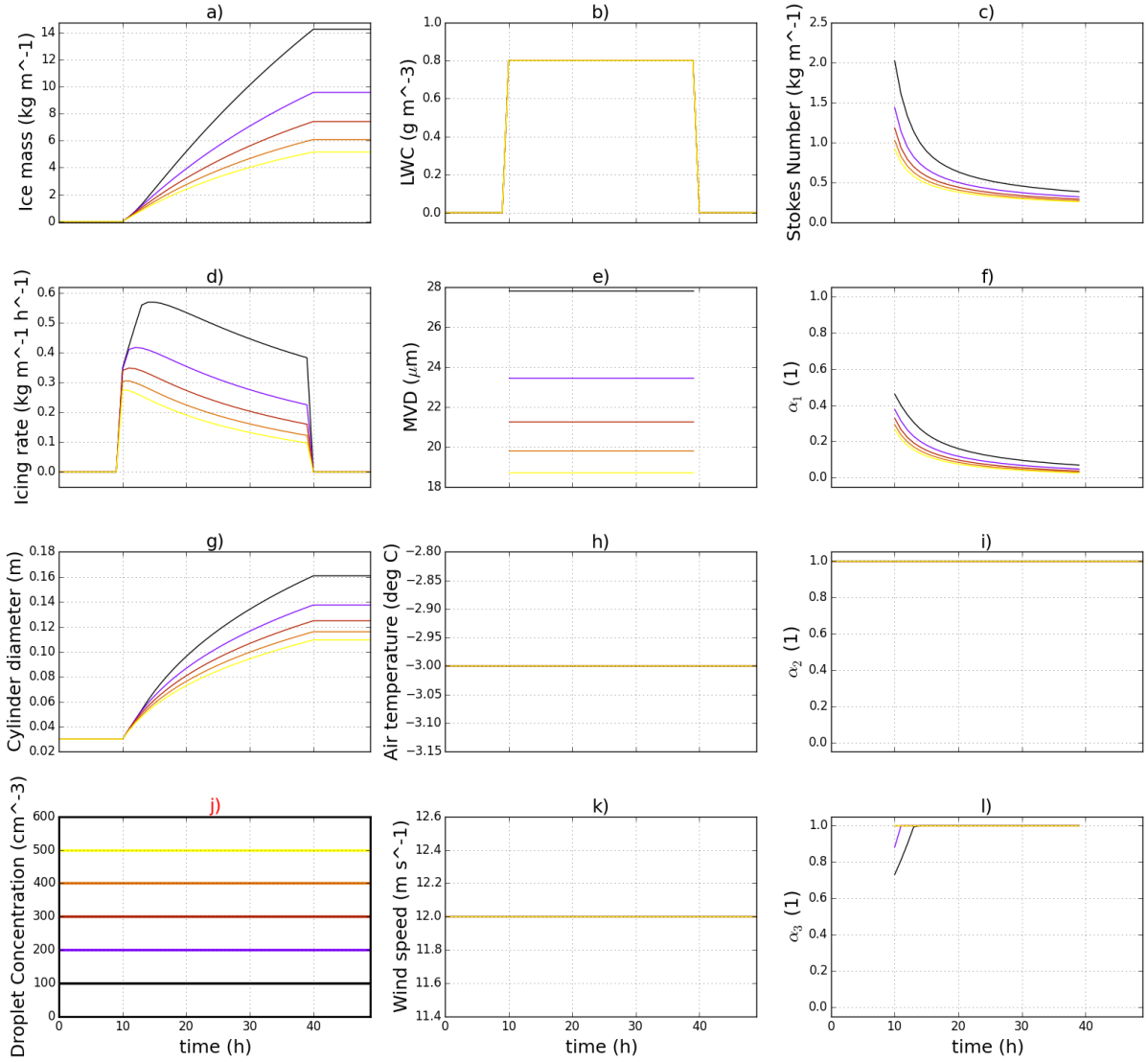


*Figure 15: The behaviour of the Makkonen model for different droplet concentrations as input parameters.*

is expressed by the higher collision efficiency. Over time, there is once again an interaction between the decreasing collision efficiency and the increasing cylinder diameter, visible in the ice rate.

The wind speed influences many terms in the heat balance equation. Some of them are of minor importance for the Makkonen model, which will be shown in section **??**. Especially for the latent energy term due to freezing, the wind speed is rather important and therefore, under consideration of the other input parameters and the collision efficiency, high wind speeds can lead to a decrease in the accretion efficiency.

Measuring the wind speed is much easier and better than it is for the droplet concentration or the LWC. Since the wind speed influences many important parameters within the Makkonen model, it is also quite responsive to small changes. Therefore, it is one of the most important input parameters too.

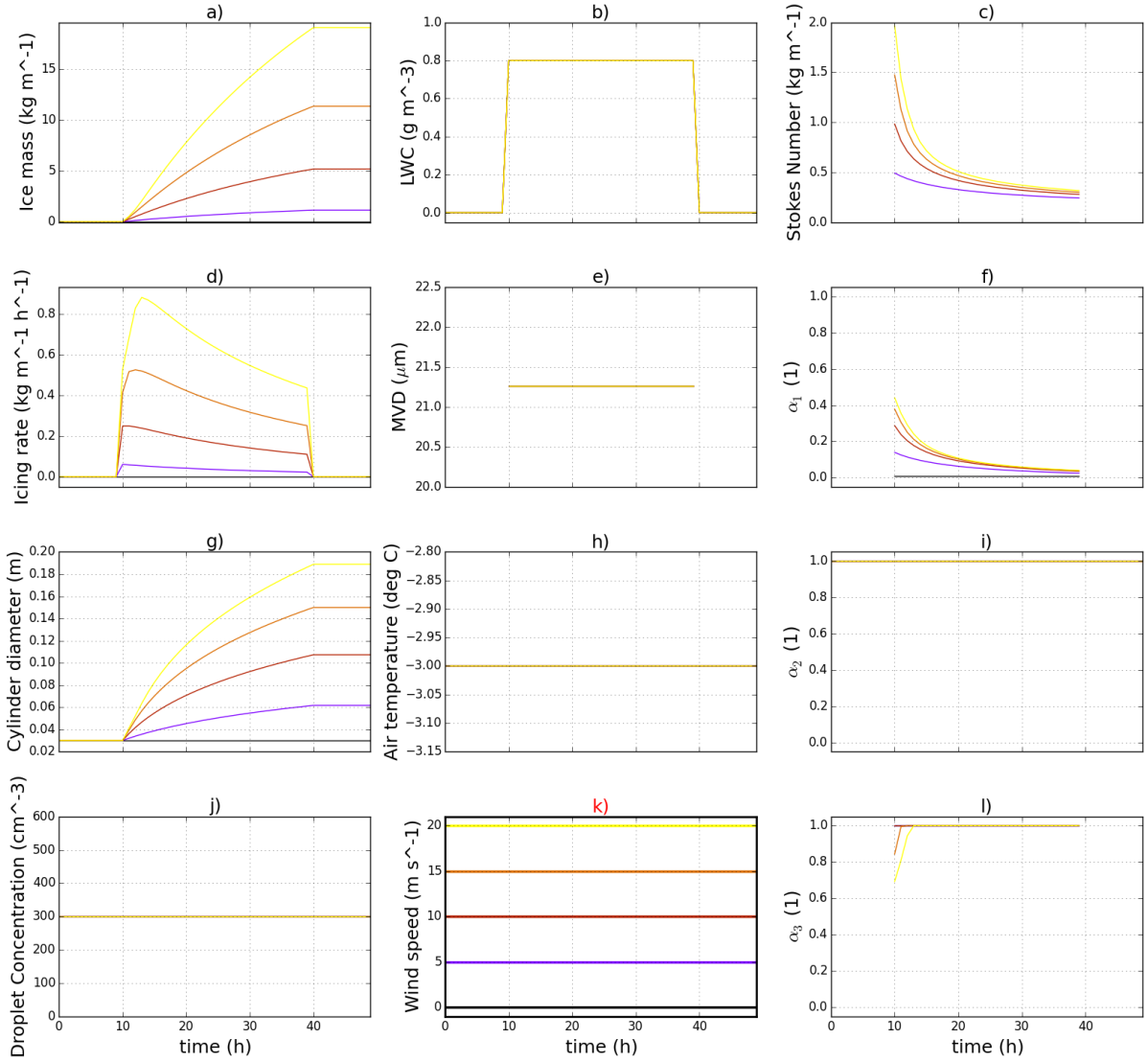


*Figure 16: The behaviour of the Makkonen model for different wind speeds as input parameters.*

**Temperature**

The temperature is another key input parameter for the Makkonen model showing a totally different behaviour than the input parameters discussed previously. Figure 17 shows the impact of different temperatures on the icing model. The black line in figure 17 h) indicates the highest temperature, which is above 0 °C. The other lines decrease linearly down to -5 °C, which is represented by the yellow line. The Makkonen model works only for temperatures below the freezing point i.e. there is no ice accretion above 0 °C. This can be seen in figure 17, where the black line shows no icing rate nor an ice load at any timestep. As a consequence, the cylinder diameter does not alter as well as the Stokes number and the collision efficiency.

The purple line represents a temperature close to the freezing point. For this temperature the model's behaviour is quite eye-catching. The reason for this is the major effect on the accretion efficiency. While the latent heat term (13) is the most important term to reduce the accretion efficiency, the evaporation term (22) and the convective heat term (21) are the biggest counterparts, which are rais-

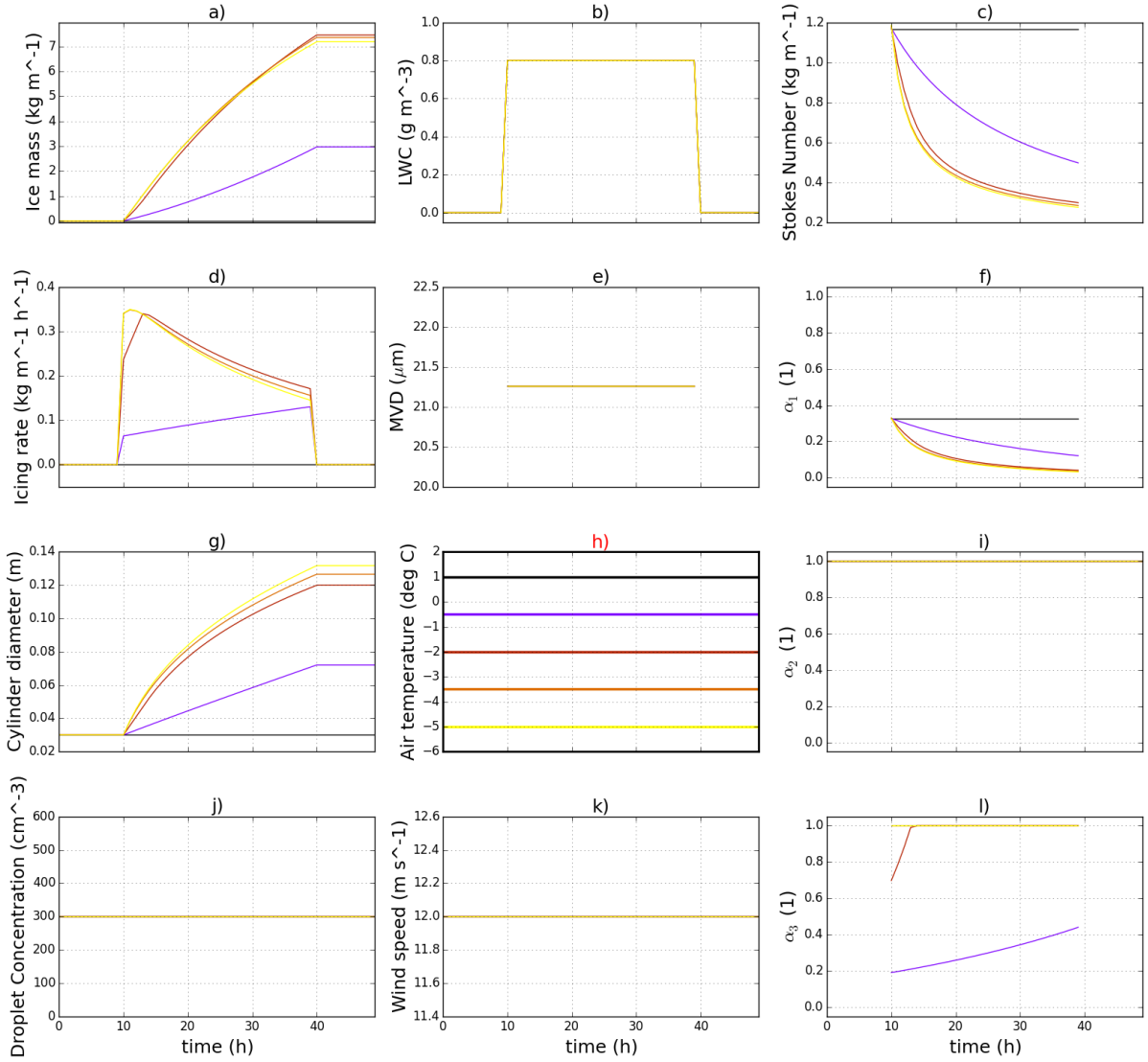


*Figure 17: The behaviour of the Makkonen model for different temperatures as input parameters.*

ing the accretion efficiency. But both terms depend strongly on the temperature. For the convective heat term $Q_c$ the impact is quite obvious and also the evaporative term only depends on the temperature, since it is assumed that during in - cloud icing the air is saturated with respect to water. If the temperature gets closer to 0 °C, the differences in these terms are also converging to zero and therefore the accretion efficiency depletes from unity. In figure 17 l), one can see the lower values of the accretion efficiency for the temperature close to 0 °C, which increases over time due to the interaction between the the decreasing collision efficiency and the increasing cylinder diameter. It should be noted that this can also happen for temperatures further away from the freezing point depending on the other input parameters, which influence the latent heat term $Q_f$, namely the LWC, the droplet concentration and the wind speed.

For scenarios with lower temperatures, such as in this case represented by the orange and the yellow line, the model behaves quite similar. This behaviour occurs, because there is no reduction of the accretion efficiency anymore and so the temperature can only impact the collision efficiency and the

density calculations. The temperature only has a minor influence on the collision efficiency, because it only effects the air density $\rho_a$, which is a variable in the equation for the Reynolds number (5). As it will be shown in section 5, the sensitivity of the Reynolds number is small compared to the other internal parameters and so the temperature effect on the collision efficiency can be neglected. The differences visible in figure 17 are only due to the small impact of the temperature on the calculations of the density, especially on the Macklin's parameter. A lower temperature produces a higher Macklin's parameter based on (27), which triggers a higher density and as a result the same ice mass produces a smaller increase of the cylinder diameter. However, this effect is also small compared to impacts shown previously.

To conclude the temperature is less important for scenarios, in which the temperature is low enough to compensate the effects of the LWC, the droplet concentration and the wind speed on the accretion efficiency. For temperatures close to the freezing point, the temperature gains a lot of importance.

**Pressure and specific humidity**

The surface pressure and the specific humidity are also input parameters for the Makkonen model but with less importance than the other parameters. The specific humidity for example is only important for the evaporative term $Q_e$ in the heat balance equation. Since the focus is on in-cloud icing conditions, it is assumed that the air is saturated with respect to water and also for precipitation events the relative humidity is rather high and close to saturation. This input parameter can only be important if evaporation is used as an ice ablation process for no icing conditions, e.g. on a sunny, windy and dry day. Nevertheless, during icing events the atmosphere is cloudy and moist. Therefore, the specific humidity is set so that the relative humidity is at 100 %.

The surface pressure has a little bit more impact than the specific humidity, but still less than the other input parameters introduced before. It can affect the evaporative term in the heat balance equation and also has an influence on the Reynolds number for the same reason as the temperature, as mentioned above. But relative changes in the surface pressure are small compared to the relative changes possible in the other input parameters and therefore changes in the surface pressure only have a little impact on the Makkonen model.

**The most essential input parameters**

To sum up, all of the input parameters apart from the surface pressure and the specific humidity are quite important and can influence the model. Especially close to the freezing point, changes in the input parameters LWC, droplet concentration, wind speed and temperature can cause big differences in the final ice load on the cylinder. Additionally, it was possible to see in the figures 14 - 17 that droplet size and wind speed are positively correlated with the collision efficiency, while big drops, high wind speeds and temperatures close to the freezing point force the accretion efficiency to become less than unity. Therefore, this thesis will distinguish between two categories:

- $\alpha_1$ **regime**: low LWC, high droplet concentration, very low temperatures and small wind speeds
- $\alpha_3$ **regime**: high LWC, low droplet concentration, temperatures close to the freezing point, high wind speeds

So under the $\alpha_1$ regime the icing prediction is dominated by collision efficiency and under the $\alpha_3$ regime it is dominated by the accretion efficiency. Although there is a big overlap between these

two conditions due to the different combinations of the input parameters, they will help to show the key concepts of the Makkonen model. Freezing rain events for example tend to be a part of the $\alpha_3$ condition category because of their droplet size.

# 5 Sensitivity of icing predictions to internal parameter perturbations

## 5.1 Methodology

**Impact on the model**

Another key aspect in this thesis is the importance and the sensitivity of the icing model to the internal parameters. As explained in section 2.2, the model contains a lot of assumptions. Therefore, perturbing the internal parameters, gives an insight into the most responsive parameters inside the icing models and how they react to small changes. The usage of adjoint models is a common aid for sensitivity studies, because they allow a quicker and cost-efficient approach to estimate the model's uncertainties (Errico, 1997). Since the empirical icing models in this thesis are low-prized regarding the computational costs, an easier attempt is used here.

As a first step the impact of the internal parameters on the resulting ice load is tested. Since the parameters inside the model depend on the input parameters, the perturbed internal parameters do as well. Therefore, each internal parameter, listed in table 5 is perturbed by a factor of +/- 10%. To account for the impact of the input parameters, these tests are run under different meteorological conditions, leading to different input parameters. While two input parameters are varied, the other parameters are again set to the constant values shown in table 4. These simulations are run for just one timestep in order to avoid interaction between each timestep, which might affect the results significantly. Finally, relative changes in the ice load are observed by perturbing the internal parameters and comparing the results to ice loads, received by unperturbed model runs.

The selection of 10% perturbations is based on tests with different perturbations (10%,20%, 30%), where the choice of the size does not change the pattern of the effects seen in the results. The ad-hoc choice of a 10% uncertainty on the internal parameters seems legitimately, regarding many of the internal parameters relying on sometimes coarse assumptions. Future works could focus on tuning the perturbations to give the best comparison with observed icing in a verification, but this is beyond the scope of this thesis. Molinder (2018) showed during a presentation in Winterwind 2018 that in her version of an ice accretion model, she only perturbs the MVD by a factor of 50%, ignoring all the other internal parameters. Since she does not distinguish between uncertainties caused by the input parameters and the internal parameters, 10% seems quite reasonable for perturbing only the internal parameters.

**Selection of the most important internal parameters**

In order to decide which parameters shall be perturbed during an ensemble forecast in future, further steps are taken. In place of using synthetic data to achieve more general results, WRF model data, which simulate real events, are taken. For different cases, related to different meteorological situations and different characteristics regarding the icing model's input parameters, the ensemble range is estimated from the resulting ice loads. The magnitude of the range is ranked manually, as shown in table 5 and as a result, the internal parameters causing the biggest ensemble range are stated to be the most important ones. The ensemble is designed by running 500 runs for the control run of the WRFMP for one icing event. For each internal parameter using a different perturbation each run over the whole time, this ensemble is calculated. The perturbation is created by multiplying a normally

distributed random number between [-1, 1] by a 10% disturbance used as a factor to the internal parameter. Conclusively, for every internal term 500 runs are simulated, where the range is represented by the envelope of the ensemble. As in the subsection 4 the focus is again on in-cloud icing only and therefore, internal parameters related to rain drops will not be perturbed within this study.

Having the most important internal parameters, an ensemble is calculated for two different cases during the winter 2016/17. This is done by perturbing the most sensitive parameters by a random perturbation between approximately [-10%, 10%], generated the same way as above, with the difference that not only one but all important internal parameters are perturbed. For these cases, the ensembles are compared and the question, whether the input parameters or the internal parameters are more important can be answered.

## 5.2 Results and Discussion

**Model sensitivity to the MVD**

Comparing the graphics for all internal parameters, one of the biggest relative changes can be found for the MVD, see figure 18. Additionally, the MVD basically depends on two rather uncertain input parameters (LWC, droplet concentration), which are used together to estimate one droplet diameter, representative for the complete droplet spectrum for a given event. These uncertainties are the reason why the MVD is sometimes the central input parameter perturbed in probabilistic models e.g. in Söderman et al. (2017).

By looking into figure 18, one can see that the sensitivity of the MVD calculations strongly depends on the input parameters, which is another prove for the importance of the LWC and the droplet concentration. Here, a rectangle represents a combination of input parameters, where the left side represents a negative and the right side a positive perturbation of 10%. It is interesting to see that especially for very small droplets, i.e. low LWC and high number of particles per volume unit, the relative changes in the icing rate are up to 40 %. This is due to the changes in the collision efficiency, because smaller droplets have a smaller $\alpha_1$, so an increase in the droplet size causes an increase of the collision efficiency. The distribution of the relative changes reflects the results from Finstad et al. (1987), stating that for very small collision efficiencies, which can be caused by very small droplets compared to the cylinder size, the fit is more error-prone. It should be noted that although the relative error of 40% is quite big, the absolute error would be rather small due to the small icing rate caused by the small collision efficiency. Another interesting point is the corner on the right side at the bottom where relative changes in the MVD equations show no effect on the icing rate. This feature will be discussed below.

**Collision efficiency $\alpha_1$ versus accretion efficiency $\alpha_3$**
In the previous paragraph, it is shown that the internal sensitivity of the MVD vanishes with increasing droplet size. This is based on the transition from the $\alpha_1$ regime to the $\alpha_3$ regime. In section 4 the $\alpha_1$ regime was defined as conditions, where the droplets are small and the wind speed is also rather low. When the droplets grow and the collision efficiency increases, the accretion efficiency starts to decrease, depending on the given wind speed and temperature. This is the point, where the $\alpha_1$ regime turns into the $\alpha_3$ regime. In figure 19, the transition from $\alpha_1$ to the $\alpha_3$ regime is clearly visible, related to the increase of the droplet diameters. The collision efficiency $\alpha_1$ is more responsive to meteoro-

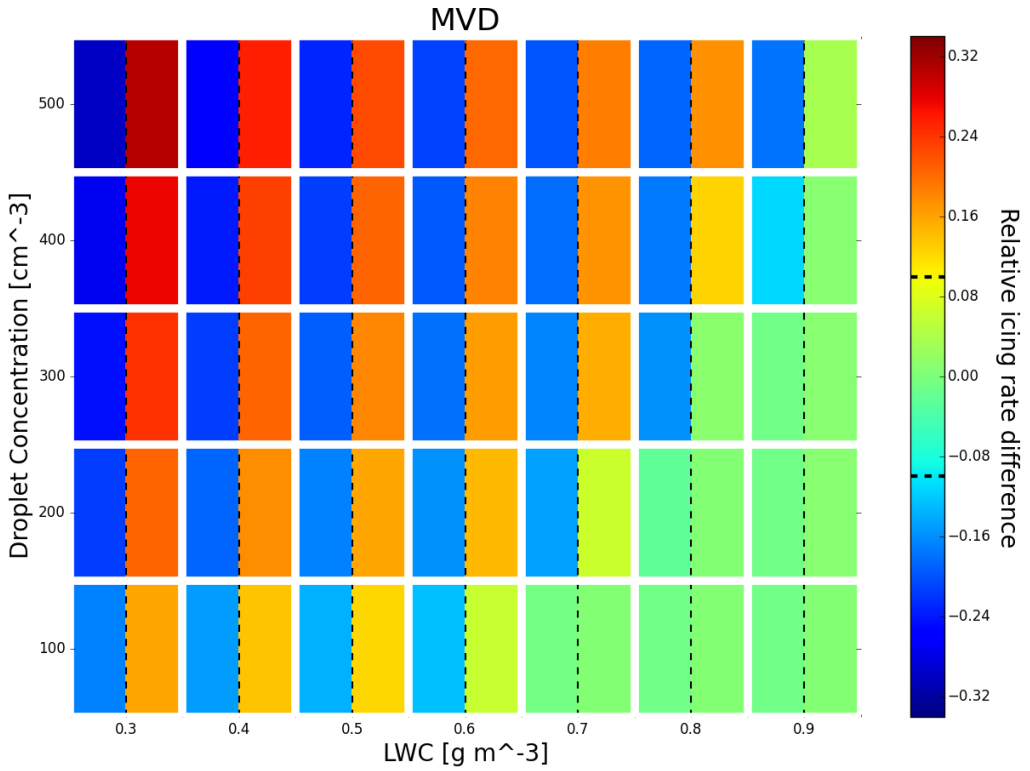


*Figure 18: Sensitivity of the Makkonen model to the MVD. The plot shows the relative changes of the icing rate for a perturbation (+/- 10 %) on the selected internal parameter under different meteorological conditions. The left side of one square represents a negative perturbation while the right side uses a positive perturbation. The black dotted line in the colorbar marks the +/- 10 %.*

logical situations based on the $\alpha_1$ regime and the accretion efficiency $\alpha_3$ is very important for input parameters of the $\alpha_3$ regime. This effect is the reason, the icing rate does not show any changes anymore for variations in $\alpha_1$, visible in the graphic at the top of figure 19. This effect happens, because an additional increase of the collision efficiency would cause an additional decrease in the accretion efficiency and as a consequence these two effects compensate each other.

There is an opposite outcome for the accretion efficiency. Using the heat balance equation (25) to calculate $\alpha_3$ , it can occur that the calculated efficiency is bigger than unity, especially for the $\alpha_1$ regime. This is because the heat balance equation is basically designed for situations under the $\alpha_3$ regime. It can be neglected regarding the $\alpha_1$ regime, because in these cases all of the liquid water will freeze immediately on the surface and the accretion efficiency will be set to unity. As a consequence, the accretion efficiency is cut down to unity for these cases, because higher accretion efficiencies would not be physically explainable. In the lower graphic of figure 19, even a reduction of the accretion efficiency of 10% can not cause values smaller than unity and therefore, they are cut down to one. As soon as the transition to the $\alpha_3$ regime takes place, the accretion efficiency gains importance and becomes more sensitive.

Figure 19 shows this behaviour for the efficiencies themselves but this can also be seen for every internal parameter related to the particular efficiencies. As an example, one can see in figure 18 that the

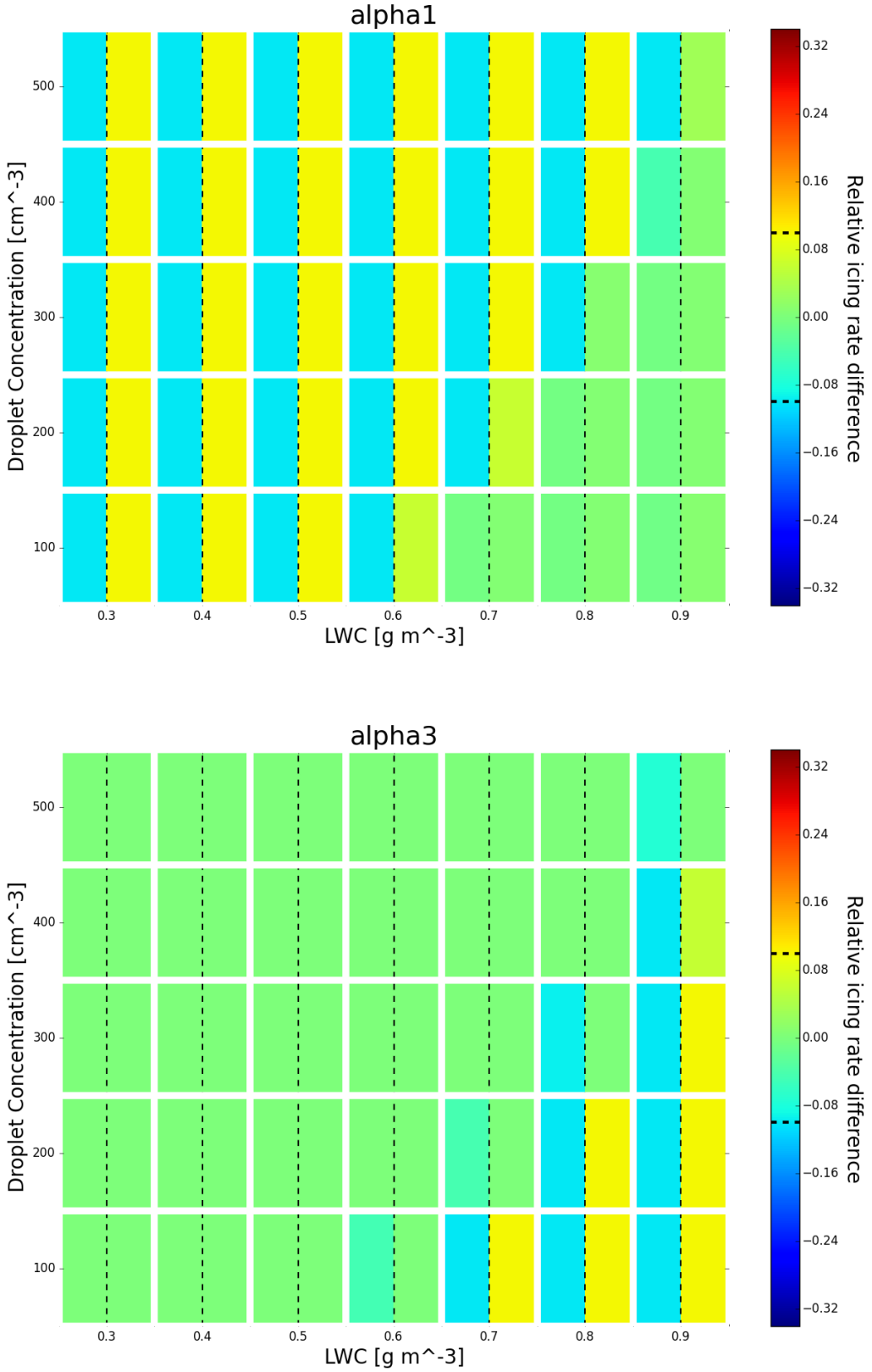


*Figure 19: As in figure 18, but for different internal parameters, showing the transition from the $\alpha_1$ regime to the $\alpha_3$ regime.*

MVD has a pattern similar to the collision efficiency because the droplet diameter is a key parameter in the calculations of this efficiency. Therefore, one can make the following conclusion. Internal parameters related to the calculations of the collision efficiency are more uncertain and important under meteorological conditions related to the $\alpha_1$ regime. The same applies to the accretion efficiency under the $\alpha_3$ regime.

**The effect of higher wind speeds**

The transition from the $\alpha_1$ regime to the $\alpha_3$ regime does not only depend on the droplet diameter but also on the wind speed. Especially regarding the iceBlade model, where extra terms are added to the wind speed, the free stream velocity can go up to 80 m s$^{-1}$. Figure 20 shows the behaviour of the model for much higher wind speeds. In this figure the transition effect is visible again, because increasing the wind speed increases the accretion efficiency and therefore less LWC is needed to reach the $\alpha_3$ regime for high wind speeds. This result can be converted to the iceBlade model, as it is done in Davis et al. (2014). Assuming that the only difference between the Makkonen model and the iceBlade model is the additional wind speed due to the rotation, one would expect rather high collision efficiencies and lower accretion efficiencies. In other words, higher wind speeds make the $\alpha_3$ regime more likely.

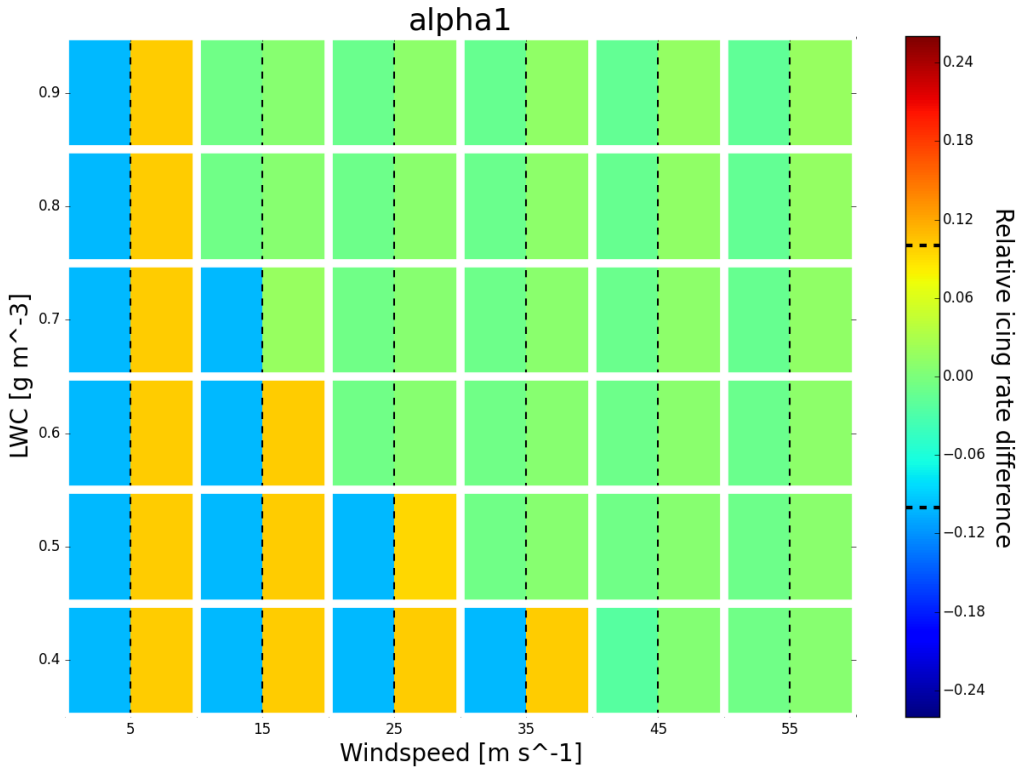


*Figure 20: As in figure 18, but for higher wind speeds, showing a shift of the transition from the $\alpha_1$ regime to the $\alpha_3$ regime.*

**The effect of bigger cylinder diameters**

Considering the iceBlade model, another essential parameter is the cylinder diameter. For the original Makkonen model, the cylinder is set to 0.03 m. But it is possible to select a different cylinder diameter and to see how the model's behaviour changes. Figure 21 gives an insight of the impact of

the cylinder diameter on the Makkonen model and also on the iceBlade model. In this figure, there are two green regions. The big green area is related to scenarios, in which the cylinder diameter is too big to cause any icing. It can be justified, because with an increasing cylinder diameter, the Stokes number in equation (3) decreases and as a consequence the collision efficiency decreases. For very big cylinders the collision efficiency is so small that it reaches its lower limit. As for the accretion efficiency, the lower limit for the collision efficiency is applied after altering the internal parameter with the perturbation. So for very big cylinder diameters even the perturbation cannot change the efficiency enough, so that a change in the icing rate is visible.

The small green area in figure 21 is represented by a high LWC compared to a relative small cylinder diameter. It shows the transition from the $\alpha_1$ regime to the $\alpha_3$ regime by increasing the LWC. As the cylinder diameter increases, the collision efficiency decreases. But due to the influence of the collision efficiency on the accretion efficiency in Eq. (14), the accretion efficiency increases. So by increasing the cylinder diameter, as it is done for the iceBlade model the $\alpha_1$ regime becomes more likely.

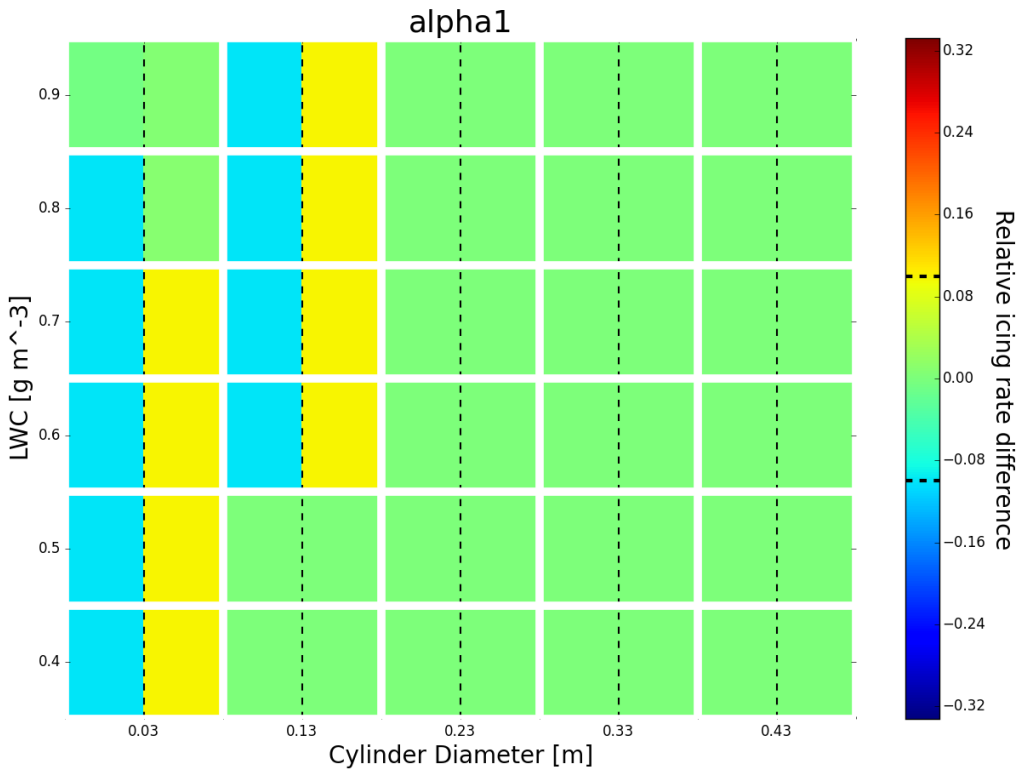


*Figure 21: As in figure 18, but for a range of cylinder diameters, showing a shift of the transition from the $\alpha_3$ regime to the $\alpha_1$ regime.*

**Conclusions for the iceBlade model**

Testing higher wind speeds and bigger cylinder diameters with the Makkonen model provides interesting results, useful to understand the behaviour of the iceBlade model. The main difference between these two models is the higher blade-relative velocity in the iceBlade model due to the rotation of the blade and the bigger cylinder representing the blade in the iceBlade model. These two

effects work in to opposite directions. While higher wind speeds support the $\alpha_3$ regime, bigger cylinder diameters aid to the $\alpha_1$ regime. The increase of the blade-relative velocity and also the size of the turbine blade strongly depends on the position of the segment on the blade. At the tip of the blade the highest velocities and also the smallest cylinder diameters are expected. Close to the root the velocity decreases and the cylinder diameter becomes bigger. Therefore, depending on the exact blade geometry, it is expected that at the tip, parameters related to the accretion efficiency are more important and by moving further away from the tip the internal parameters related to the collision efficiency gain importance. At a certain distance away from the tip, the cylinder diameter might be too big and as a result there is no significant icing anymore, comparable to the big green area in figure 21 for the Makkonen model.

**Sensitivity of the Makkonen model for real cases**

Knowing the general results, explained previously, the Makkonen model is tested under more realistic conditions based on the measurements from the winter 2016/17 for a wind farm in Ellern. Different icing events are selected and then each internal parameter is ranked based on the magnitude of the range of the resulting ice load. Due to the small number of icing events available, there is only one event having a significant icing rate, which can be seen in figure 11, where only the icing event at the beginning of January shows a moderate ice growth. Therefore, 03/04 Jan 2017 is selected to represent the importance of internal parameters related to the $\alpha_3$ regime, because the higher icing rate goes along with an increased wind speed and a higher LWC. For the importance of internal parameters related to the $\alpha_1$ regime three lighter icing events, similar to the event on 24/25 Jan 2017, are chosen. The results of the evaluation can be seen in table 5.

As expected, the internal parameters related to the computations of the MVD show the biggest ensemble range and they are consequently the most sensitive parameters under the $\alpha_1$ regime. Therefore, these results also support the choice of perturbing the MVD in Molinder (2018). Another interesting point regarding the internal parameters related to the $\alpha_1$ regime is the small ensemble range generated by the Reynolds number. This insensitivity of the Reynolds number in this model allows neglecting the influence of the temperature through the air density concerning changes in the collision efficiency, as described in 4.

Looking at the internal parameters related to the $\alpha_3$ regime such as the convective heat-transfer coefficient or the latent heat of freezing, one can see that the most important terms are ranked behind the most important internal parameters related to the $\alpha_1$ regime. This is probably caused by the lack of really severe icing events in Ellern during the winter 2016/17. By assuming that this winter is representative of all winters in Ellern, the fundamental internal parameters related to the computations of the collision efficiency are more important than the others.

The green highlighted internal parameters in table 5 show the selection of the most important parameters, which are perturbed in all further simulations. Since the models are very cost-efficient, parameters until rank 4 are selected. Nevertheless, it should be kept in mind that the real impact of the internal parameters depends on the meteorological conditions. So under the $\alpha_1$ regime the Stokes number, which has the rank 3, can be more important than the latent heat due to freezing, for example.

| Internal parameter | Related equation | Rank | Important for |
|---|---|---|---|
| Slope of the distribution $\lambda$ | (7) | 1 | $\alpha_1$ |
| MVD $d$ | (8) | 1 | $\alpha_1$ |
| Fitting parameter $A$ | (10) | 2 | $\alpha_1$ |
| Collision efficiency $\alpha_1$ | (9) | 2 | $\alpha_1$ |
| Convective heat - transfer coefficient $h$ | (19) | 2 | $\alpha_3$ |
| Latent heat due to freezing $Q_f$ | (13) | 2 | $\alpha_3$ |
| Accretion efficiency $\alpha_3$ | (25) | 2 | $\alpha_3$ |
| Stokes number $K$ | (3) | 3 | $\alpha_1$ |
| Convective heat transfer $Q_c$ + longwave radiation $Q_s$ | (25) | 3 | $\alpha_3$ |
| Heat transfer due to evaporation $Q_e$ | (22) | 4 | $\alpha_3$ |
| ice density $\rho$ | (26) | 4 | / |
| Fitting parameter $B$ | (10) | 5 | $\alpha_1$ |
| Fitting parameter $C$ | (10) | 5 | $\alpha_1$ |
| Shape parameter $\mu_s$ | (6) | 5 | $\alpha_1$ |
| Aerodynamic heating $Q_a$ | (16) | 5 | $\alpha_3$ |
| Heat transfer due to the impinging droplet $Q_l$ | (23) | 5 | $\alpha_3$ |
| Macklin's parameter $R$ | (27) | 5 | / |
| Reynolds number $Re$ | (5) | 6 | $\alpha_1$ |
| Kinetic heat transfer $Q_v$ | (15) | 6 | $\alpha_3$ |
| Fitting parameter $K_0$ | (28) | 6 | / |
| Droplet impact speed $v_0$ | (29) | 6 | / |

*Table 5: Available internal parameters related to in-cloud icing, where the related equation refers to the term, in which the perturbation is placed. The last column assigns the internal parameters to their corresponding efficiencies, if existent. They are sorted by their rank based on the size of their possible range in the Makkonen model, explained in section 5. The green highlighted parameters represent the most important parameters, which are used to establish an ensemble. Note the increasing importance of $Q_a$ in the iceBlade model due to the higher blade-relative velocity.*

Also, the aerodynamic heating is included in the list of important internal parameters, even though it is ranked fifth. This parameter shows another big difference between the iceBlade and the Makkonen model. For the Makkonen model this term has no impact and therefore perturbing it will not change the resulting ice load significantly. Still, there are two big differences for the iceBlade model, one is the bigger cylinder diameter and the other is the increasing blade-relative velocity. The former has only an impact on the convective heat-transfer coefficient. The latter can change the importance of this term completely. In equation (16), the wind speed, in this case the blade-relative velocity, is squared, so an increase in this variable can increase the energy term quite a lot. Additionally, the convective heat - transfer term also increases with increasing velocity. Therefore, especially for the tip of the blade, where the blade-relative velocity is high and the cylinder diameter rather small, perturbing this internal parameter can change the ice load significantly. This is the reason, why the aerodynamic heating term is also included in the list of the most important internal parameters.

Finally, two case studies are presented.

**Case 1: 3 Jan 2017 - 5 Jan 2017**

Case 1 represents the strongest icing event for the wind farm in Ellern starting on 3 Jan 2017. Figure 22 shows boxplots for the ensembles based on the Makkonen model. The left side is an ensemble icing forecast forced by the WRFMP ensemble members, shown in table 3. The right column shows an ensemble icing forecast forced by the WRFMP ensemble members, subject to internal parameter perturbations. The resulting probabilities are compared with the IceMonitor, but due to the many observed issues of the IceMonitor, described in section 3.1, the observations are only used as a guideline and should be treated with caution.

Starting with the left side, one can see that all ensemble members in the WRFMP ensemble predict icing but with different severities. The important time interval is between 1800 UTC 3 Jan 2017 and 0600 UTC 4 Jan 2017, here the icing rate has the biggest amplitude. Differences, especially in the predicted LWC cause different icing rates and lead to different ice loads, hence the resulting ice load has a rather large spread. Nevertheless, the prediction is quite good, because the observed ice load is within the blue box, close to the median.

The result for the right side, including internal perturbations, is also quite good. Again, the observations are close to the median and inside the blue box. Comparing both ensembles, the quartiles do not change a lot by including internal perturbations, but perturbing the internal parameters increases the ensemble range, so the 5% and the 95% percentile are further away from the median and there are also many outliers up to much higher ice loads. Hence still, all ensemble members show icing. Comparing these two ensembles with the observations, both predict the ice load very well, but using only the input perturbations would be enough.

**Case 2: 24 Jan 2017 - 26 Jan 2017**

In figure 23, one can see that the predicted ice load, based on the small icing rate, is much lower than the observed ice load. Starting again with the left side, the probability box is much smaller than the box in case 1. This implies that the differences in the input ensemble are much smaller than they are in the other case. Assuming that the observation is credible, this means that none of the ensemble members are capable to predict a suitable ice load. Most of them do not predict icing at all.

Including perturbations in the internal parameters leads to similar results. The median also predicts no icing, but as in case 1 the ensemble range is larger, based on the position of the 95% percentile and the outliers, which are much closer to the observation. Therefore, using additional internal perturbations seems quite promising.

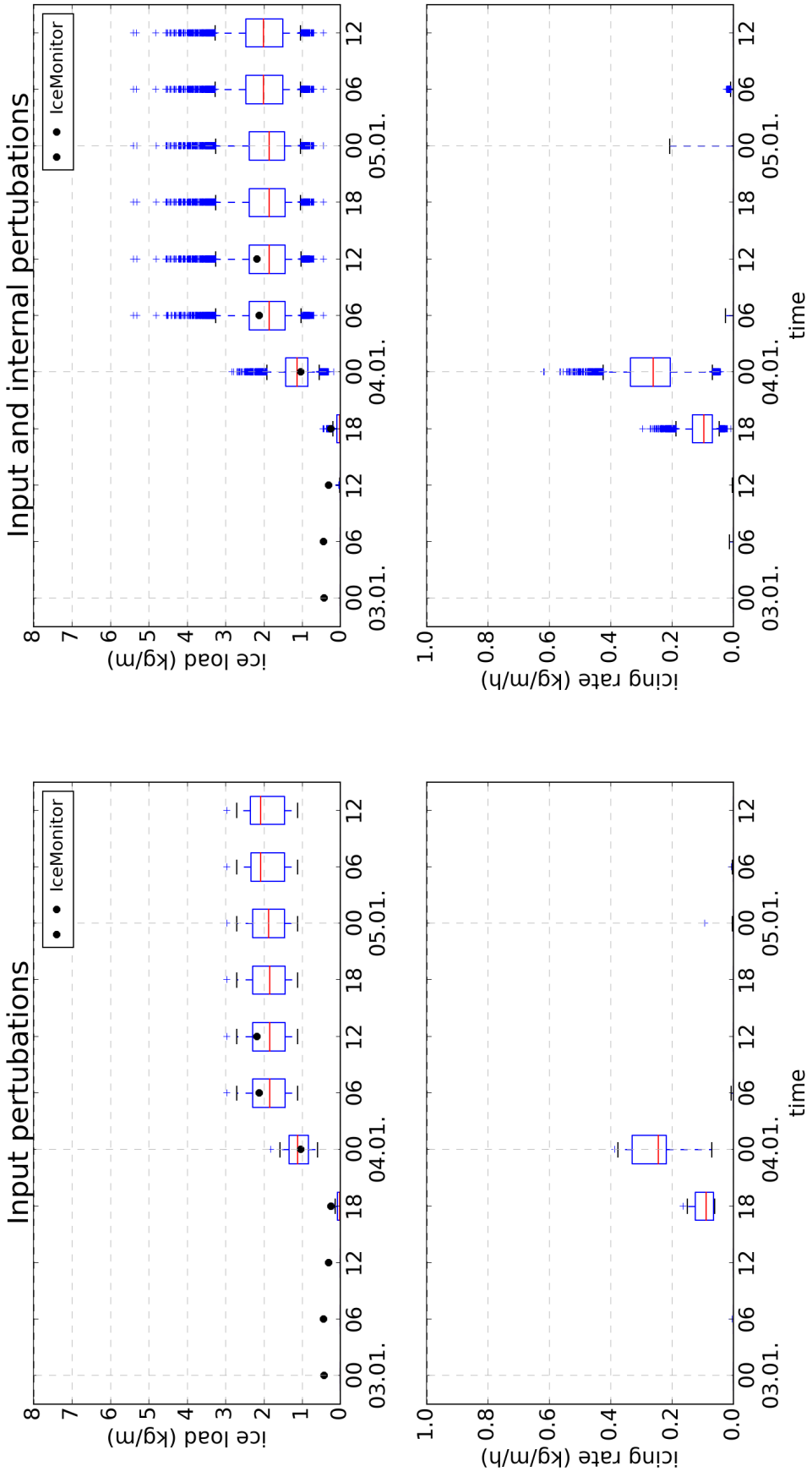


*Figure 22: Makkonen CASE 1: Boxplot comparing the ice load and the ice rate to the IceMonitor for 3 Jan 2017-5 Jan 2017. The red line is the median, the blue box shows the lower and the upper quartiles and the black horizontal line the 95% or 5% percentiles.*

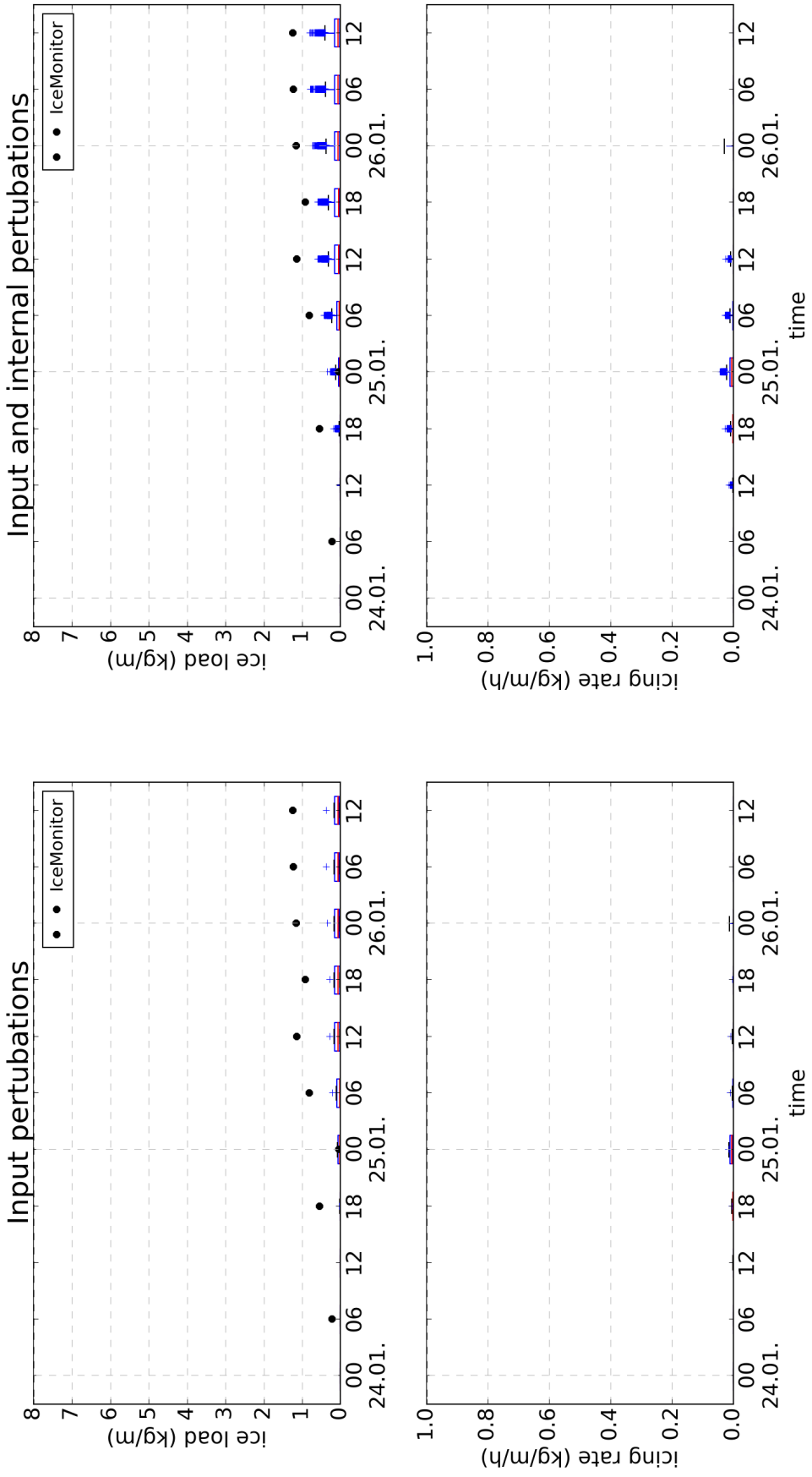


*Figure 23: Makkonen CASE 2: Boxplot comparing the ice load and the ice rate to the IceMonitor for 24 Jan 2017-26 Jan 2017. The red line is the median, the blue box shows the lower and the upper quartiles and the black horizontal line the 95% or 5% percentiles.*

Looking at both cases, precious results can be obtained. First of all, the internal perturbations strongly depend on the input parameters. In both cases, one can see that the range is enlarged, but the medians of the predicted ice loads are always similar to each other. This is not a big surprise, since the sensitivities of the internal parameters depend on the input parameters as well. As a consequence, using internal perturbations has no additional value, compared to using only an input parameter ensemble, regarding binary decisions, whether icing occurs or not using a probability threshold of 50%. Because, if none of the WRFMP members have a LWC greater than zero, the internal perturbations will not change the result. The only reasonable application for using internal perturbations are categorical ice loads, because the additional spread can raise the probability for certain categories at the edge of the input parameter ensemble, just by adding internal perturbations. Whether this really improves the quality of the ensemble or just reduces the accuracy of the input parameter ensemble, can only be answered by making a quantitative ensemble verification. Due to the small amount of icing cases available for the moment, it cannot be done in the scope of this thesis.

This dependency of the internal parameters on the input parameters is also the reason why the input parameters are more important than the internal parameters, although there are situations where the ensemble range caused by the perturbed internal parameters matches the range due to the input parameter ensemble, especially if the input parameter ensemble members are rather similar. But then again, the magnitude of the internal perturbed ensemble range depends on the input parameters inside the perturbed run. Finally, the input parameters are the more important parameters, because they do not only impact the icing models, but also the internal perturbations, while the internal perturbations do not effect the input parameters. As a result in order to make a high-quality ensemble, it is essential to include perturbations in the input parameters, as for example in the WRFMP, even though it is computationally expensive. Albeit the additional value of using internal perturbations is not clear yet, the use of these perturbations can be achieved because of their low computational price.

# 6 Makkonen and iceBlade icing predictions for real cases

## 6.1 Methodology

In section 2.2.2, the iceBlade model is introduced as a transition from a static cylinder rotating around its vertical axis to a cylinder being used as a representative blade, shown in figure 9. While Davis (2014) only uses one segment of the whole blade at 85% of the blade's length, this thesis goes a little bit further and tries to predict icing along the entire blade. Therefore, the blades of the wind turbine in Ellern, mentioned in section 1.2 are used, having a length of 63 m.

Another crucial key is the representation of the cylinder diameter for each segment. Due to the lack of information of the detailed geometry of the blade, a rather coarse approach is used. The cylinder diameter is assumed to increase linearly towards the root, having a cylinder diameter of 3 cm at the tip and 3.6 m close to the root. Using this approach and partly because it is a different turbine, the cylinder diameter at 85% of the blade's length would be 53.1 cm, which is quite larger compared to the 14.4 cm in Davis (2014). Nevertheless, having this information and the operational wind data, it is possible to calculate all necessary parameters, e.g. the blade-relative velocity, to predict icing along a blade using the iceBlade model.

Explaining the iceBlade model in section 2.2.2, it was mentioned that the iceBlade model is based on the same equations as the Makkonen model. Since the Makkonen model was primarily created to predict icing on a small cylinder instead of a real wind turbine blade as used here, additional adjustments are needed, especially regarding the empirical fit for the collision efficiency $\alpha_1$. As described in section 2.2.1, the approximation function for $\alpha_1$ is accurate for the Langmuir parameter $\Phi$ between 100 and 10000 and a Stokes number between 0.17 and 1000. Figure 24 shows the relationship between these two non dimensional parameters to the collision efficiency, where the blue framed area represents the region of validity for the empirical fit in the Makkonen model. By looking at Eq. (4), the Langmuir parameter increases with an increasing blade-relative velocity (in (4) represented by the wind speed $v$) and with an increasing cylinder diameter. Since in the iceBlade model the blade-relative velocity is used instead of the wind speed and because the cylinder diameter of the turbine blade, especially closer to the root, is much larger than the cylinder diameter of the original Makkonen cylinder, the Langmuir parameter can easily exceed the limit and reach values up to 70000. Also the lower limit for the Stokes number is not practicable anymore. In the Makkonen model the lower limit is set to 0.17 to avoid negative values for the collision efficiency, what can be seen in figure 24 by the change from the white to the red area. However, for higher $\Phi$ the border between these areas is shifted to higher Stokes numbers. As a consequence the limitations used in the Makkonen model are omitted in this version of the iceBlade model and instead of that, another lower boundary is defined:

$$\alpha_1 < 0.05 \qquad \Longrightarrow \quad \alpha_1 = 0$$

Using this new restriction as the lower limit of the collision efficiency has the following advantages. First negative values of $\alpha_1$ are excluded. In contrast to the Makkonen model, the lowest limit is not set to 0.01 but to zero because by keeping this limit, unrealistic high ice loads can occur at the blade close to the root due to the increased blade-relative velocity and the larger cylinder diameter, which both affect the ice rate in equation (2). Choosing 0.05 as a threshold has two reasons. As already mentioned

in section 2.2.1 looking at the collision efficiency, the empirical fit is more error-prone for very small collision efficiencies and therefore, the errors made by setting it to zero might be negligible. But the more important reason is to avoid a non-physical behaviour of the model due to the fit. By looking again into figure 24 one can see that for the Makkonen range of validity the lines of $\alpha_1$ increase linearly. But for higher $\Phi$ the borders, especially for smaller collision efficiencies, become non linear and showing an increasing curvature. This non-linearity can cause an not wanted behaviour, which will be shown by the following thought experiment using again figure 24. Imagine having meteorological conditions in way that, the Stokes number $K$ is approximately 0.2 and the Langmuir parameter $\Phi$ is around 30000. Now it is assumed that the lower limit for $\alpha_1$ is 0.01, so by having these dimensionless parameters the collision efficiency would be 0.01. Now imagine the blade-relative velocity is increased by 50 %. In the Makkonen model an increase in the wind speed would always lead to a higher collision efficiency due to the higher Stokes number, as shown in section 4. According to the equations for the Stokes number (3) and the Langmuir Parameter (4) an increase of 50% in $v$ will also increase the dimensionless parameters by 50%, so in the end the updated $\Phi$ would be 45000 and the new $K$ would be 0.3. But by looking into figure 24 one can see that due to the strong curvature the value for the collision efficiency would decrease. This is an unpleasant behaviour and therefore, the limit is set to 0.05, which is still not a perfect straight line but using this limit it is possible to cope with this issue. Nevertheless, it should be noted that although the fit provides reasonable results with this new limitation, it was not built to estimate the collision efficiency for such big cylinder diameters and therefore it might lack in accuracy.

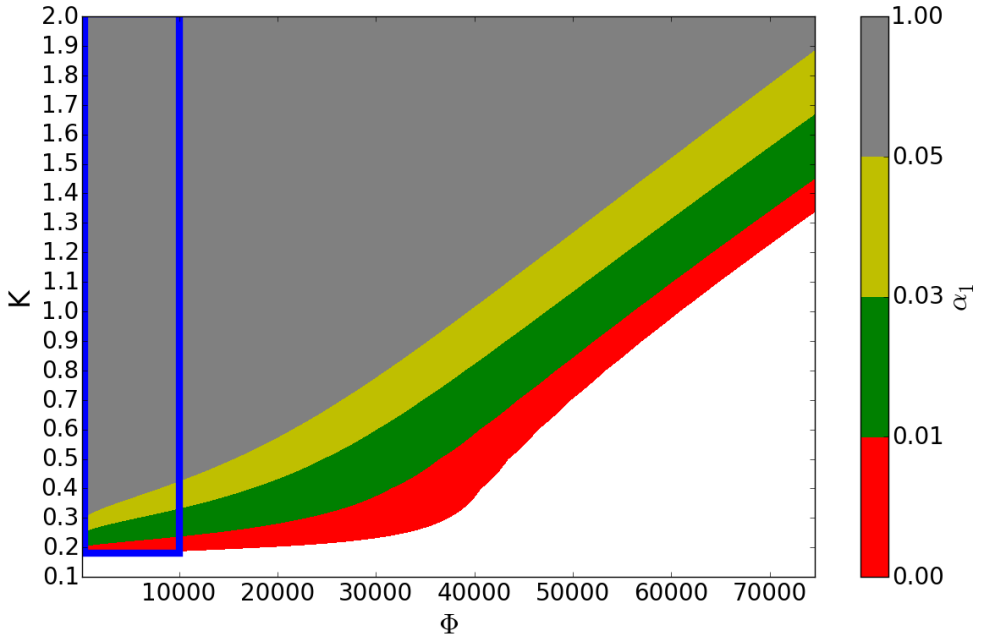


*Figure 24: Impact of the Stokes number $K$ and the Langmuirs Parameter $\Phi$ on the collision efficiency $\alpha_1$ based on the empirical fit from Finstad et al. (1987). The blue frame shows the range of validity for the empirical fit in the Makkonen model.*

After adapting the original iceBlade model using the new assumptions, case studies for two real cases are made and afterwards verified by the eologix sensors as well as by the SCADA data. Moreover, the different ways of detecting icing, introduced in section 3.1, are compared in order to estimate the quality of the predicted icing by the iceBlade model and to find improvements in the model. To pre-

dict the ice load an ensemble approach is applied, with perturbations based on the input parameters by using the WRFMP and perturbations based on the most sensitive internal parameters obtained by the results in section 5. For every member of the WRFMP ensemble, 500 internally perturbed runs are made.

Since the iceBlade model in the version used in this thesis is only an ice accretion model, there is no ablation process. In order to take into account such processes as blade heating or natural warming of the blade, an artificial ice ablation process is attempted based on the eologix sensors measured temperatures. Whenever the measured temperature is higher than 0 °C for over 50% of the eologix sensors on the leading edge, the ice is thrown off. It should be noted that this approach is only valid for the iceBlade model, because in this model the cylinder diameter is not updated every time step. Therefore the time steps do not correlate with each other and can be treated individually. The Makkonen model adjusts the cylinder diameter in every iteration and therefore the time steps correlate with each other. As a consequence, there is no ablation process used for the ice load based on the Makkonen model.

## 6.2 Results and Discussion

In this subsection, the behaviour of the iceBlade model under real icing conditions is determined for two case studies. These cases are based on the thesis from Schneider (2017) and were classified into two categories:

- Case 1 (2 Jan 2017 - 4 Jan 2017): Camera images show an ice load greater or equal to light-moderate and the SCADA data record icing.
- Case 2 (8 Nov 2016 - 10 Nov 2016): Camera images show an ice load greater or equal to light-moderate, but the SCADA data do not record icing.

Analysing these two case studies allows to investigate the necessity of predicting icing directly on the wind turbine blade and the importance of an accurate representation of the rotor blade. Additionally it gives a rough comparison between the different ice detection instruments used in this thesis. Furthermore, conclusions about the quality of the iceBlade model and future improvements can be made.

#### Case 1: 2 Jan 2017 - 4 Jan 2017

Each case study is arranged in the following way. After discussing the observations for this case, the model results based on the iceBlade model are analysed. Finally, a discussion comparing them is given. First of all, a short explanation of the following figures is presented, starting with the observation plots shown in figure 25 and figure 27:

- The first subplot shows the ice signal (green areas) measured by the different eologix sensors on the leading edge of the blade. They are sorted by their distance to the root.
- The ice signals are related to the ice thicknesses introduced in section 3.1 and the grey areas represent missing values.

- The black background color shows, when the SCADA system registers icing and as a result the blade is heated, represented by the red background colors.
- The last two rows show the reference ice detection on the hub, based on the camera images introduced in section 3.1. The comparison of the camera images with the eologix sensors allows establishing the differences between the icing on the blade and the nacelle.
- In the second and third subplot measurements from the SCADA system and the Rotronic sensors are illustrated. For the wind speed (blue line) an additional quality control flag is plotted, representing situations, in which the measured wind speed should be treated with caution.

The figures 26 and 28, representing the results obtained by the iceBlade model, include the following features:

- The first subplot shows the predicted ice loads by using ice classes for different positions along the blade (y-axis). The ice signals are calculated similar to the ice signals in the eologix sensors. For each position the cylinder diameter and the ice load for every step is taken and by assuming a density of 300 kg $m^{-3}$, the ice thickness is estimated. The ice load is assumed to be homogeneously distributed around half of the representative blade cylinder. This means that the ice signal not only depends on the ice load, but also on the cylinder diameter, because the same ice load causes a bigger ice thickness around a 3 cm cylinder than around a 3 m cylinder. For the smallest ice signal, a minimum ice load of 0.005 kg $m^{-1}$ is used.
- The prediction for each position consists of two lines. The upper line for each position shows the control run, as it is done for the observations e.g. in figure 25. The second line uses the whole ensemble and shows how many of the ensemble members are within a certain ice class. For example, for the position 55 m away from the root in figure 26, 100% have an ice signal of 2 or higher, around 75% predict ice signal 3 and 25% have an ice signal of 4.
- The blue triangles mark time steps, where at least one member of the WRFMP predicts icing due to rain drops.
- The last row of the first subplot shows a reference forecast by modelling icing on the Makkonen cylinder on the hub.
- The second and third subplot show the meteorological parameters of the whole ensemble. The bold line is the control run and the transparent area shows the envelope of the ensemble for each parameter.

Case 1 again represents the significant icing event already introduced in the section 5. This can be seen in figure 25, where the MT ice load reaches level 3 at the end of the period. It is easy to see that for the leading edge, the blade heating works almost perfectly, except the sensors on the winglet, which remain iced during the heating process. Similar to the artificial ablation process for the modelled ice load, if the eologix sensor temperature is higher than 0 °C, the ice is assumed to be thrown off. This is done, especially for ice signal 2, to distinguish whether the surface is simply wet or there is a very thin ice layer. This means that for the sensors on the winglet the eologix sensor measured temperatures are below 0 °C, even though the blade is heated. Additionally one has to keep in mind that the heating only affects the rotor blade, so for instruments placed on the hub the ice would persist.

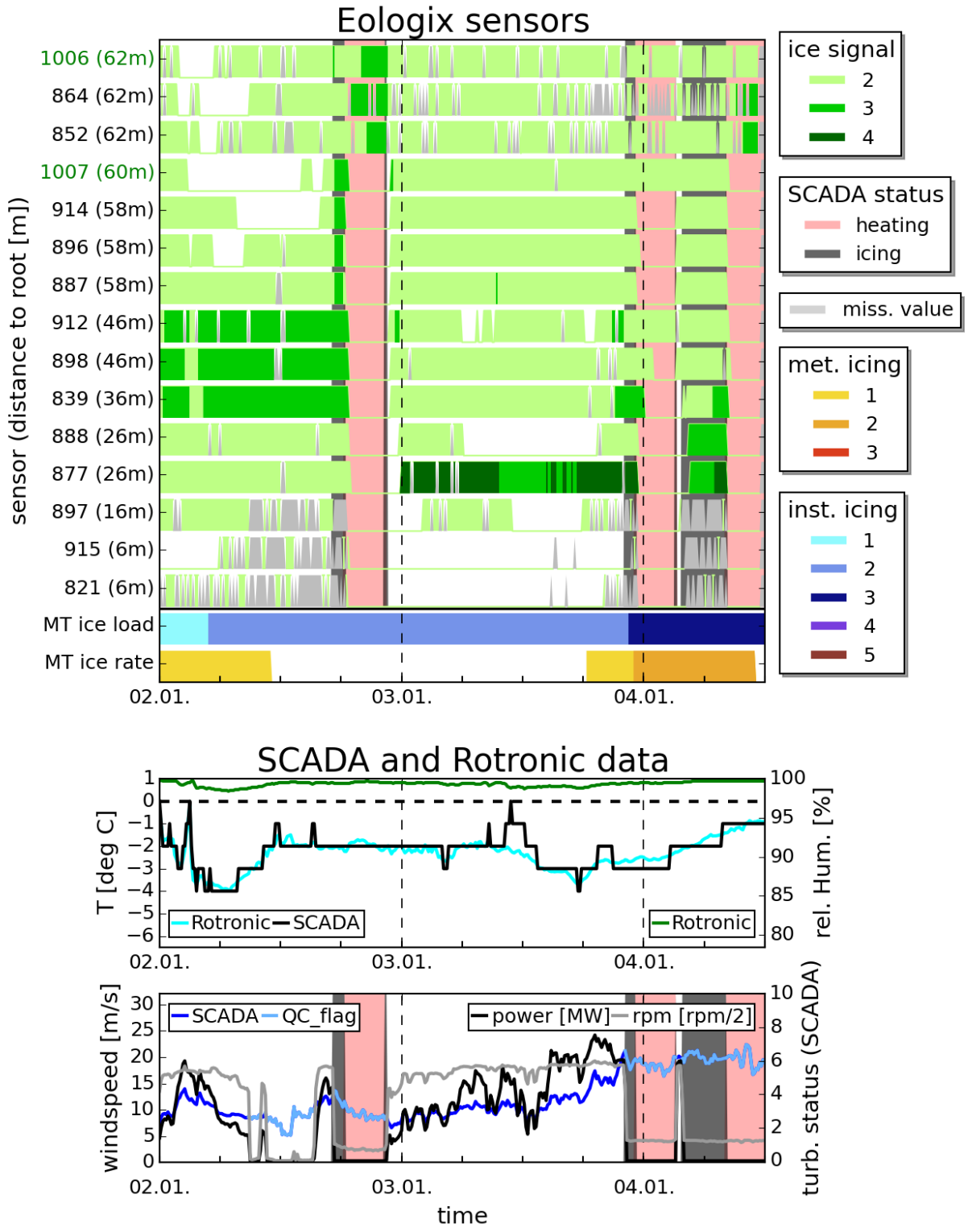


*Figure 25: iceBlade CASE 1: Overview of the observations made in the ICE CONTROL project for a wind turbine at Ellern from 0000 UTC 2 Jan 2017 to 1200 UTC 04 Jan 2017. Details are explained in section 6.*

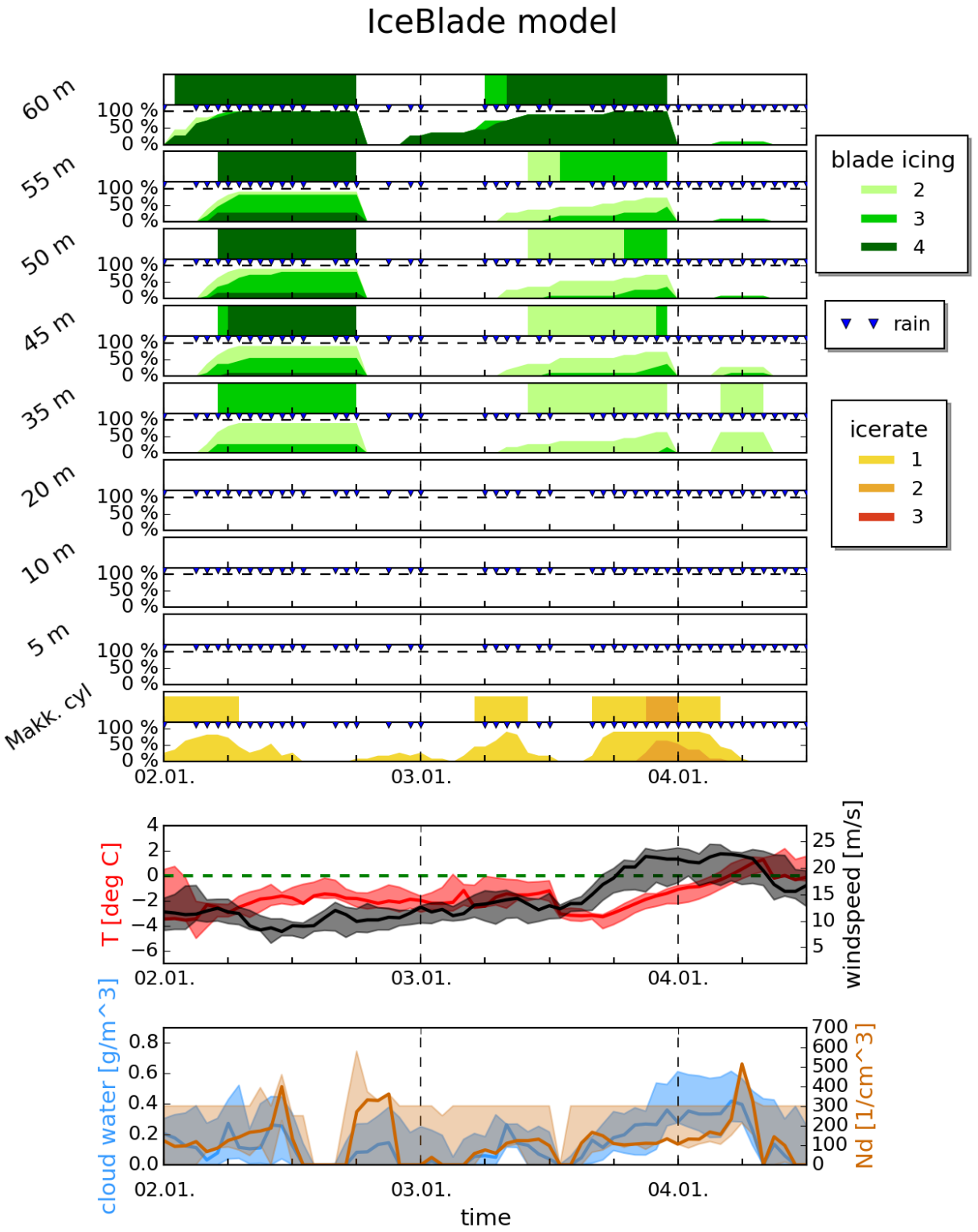


*Figure 26: iceBlade CASE 1: Icing prediction made by the iceBlade model for a wind turbine blade using an ensemble approach from 0000 UTC 2 Jan 2017 to 1200 UTC 04 Jan 2017. For each member of the WRFMP, 500 internal perturbed runs are computed. For comparison, the ice rate based on the Makkonen model is included. Details are explained in section 6.*

The relative humidity measured by the Rotronic sensor is always very close to 100%, which is a precursor for icing at the nacelle. Moreover, the temperature is always below 0 °C and the wind speed is always higher than the cut-in speed, meaning that, if there is LWC due to cloud or rain droplets, icing can occur. For the first icing event, starting on 2 Jan 2017, the correlation between the eologix sensor and the SCADA data is rather good. Having a wind speed close to 10 m $s^{-1}$ and a temperature slightly increasing to -2 °C, the ice load increases steadily until most of the eologix sensors, except the sensors on the winglet and close to the root, reach ice signal level 3. The SCADA system registers icing and after turning on the heating, the surface temperatures exceed 0 °C and the surface is supposed to be ice free. But immediately after the heating period the eologix sensor temperatures fall below 0 °C again and the sensors register light icing. This can occur, because not all ice on the blade is lost during the heating process and also because additional icing is happening. Measurements of the surface temperature, not shown here, reveal that the surface temperature of the rotor blade after the first heating period is close to 0 °C meaning that the ice type, based on figure 5, tends to be glaze. As briefly described in section 2.1.2, glaze ice has a smaller impact on the blade's aerodynamics than rime ice and this might be the reason that the light icing registered by the eologix sensors does not have an impact on the power production. At the end of the period, one of the strongest icing events, in the winter 2016/17 for the wind farm in Ellern, takes place. With a light decrease in the temperature to -3 °C, a significant decrease of the surface temperature and an increase in the wind speed, the SCADA data imply icing, although the ice signal of most eologix sensors were at level 2. Nevertheless, due to the long ice accumulation, there might be enough icing to show a significant impact on the blade's aerodynamic, maybe even caused by the creation of horns, mentioned in section 2.1.2. The last icing event, starting around 0300 UTC on 4 Jan 2017, shows that the icing conditions were rather strong so that after heating the blade, the surface temperatures fall immediately below 0 °C and the blade accretes ice again. In the end of this case period the temperature of the ambient air starts to increase steadily.

The camera images used as reference for icing at the nacelle show similar results. There are also two main events having a significant icing rate, where the second one is much stronger, visible in figure 25. Since the heating does not affect the nacelle, the ice load increases constantly during the whole time period.

The corresponding model prediction using the iceBlade model, is shown in figure 26. As already mentioned, in-cloud icing is supposed to be the prevailing mechanism of icing for the wind turbine in Ellern, as it is in this case, but only for the positions located at 60 m and 55 m apart from the root. Because due to the decrease in the blade-relative velocity and the increase in the cylinder diameter for inner positions, the collision efficiency becomes too small and as a result there is no icing due to in-cloud icing anymore. But for rain drops, a constant droplet diameter of 100 $\mu$m is assumed and therefore, the collision efficiency is still greater than zero. For the positions close to the tip, in-cloud icing clearly has a bigger impact than icing due to rain drops. This is because for rain drops the smaller accretion efficiency reduces the icing significantly. For positions, where the cloud droplets are too small, rain drops are the only mechanism left in this model to accrete ice. Very close to the root, no icing is predicted at all, because the cylinder diameters are too big and the blade-relative velocities too small to have a collision efficiency greater than zero.

By using the artificial ablation the iceBlade model predicted ice classes having a good timing compared to the observations from the eologix sensors. The intensity is very different and might also be

caused due to the coarse representation of the blade geometry. Also, the ice rate on the Makkonen cylinder is very similar to the observations made with the cameras, with the difference that in the model there is also an icing rate in the morning of 3 Jan 2017, which is not observed. The biggest difference occurs at the end of the time period. While observations show a significant icing after heating the blade, the model has only slight icing close to the middle of the blade. This is mainly caused by the difference in the temperature. While in the observations the temperature reaches -1 °C, most of the runs in the model predict the temperature increase earlier and therefore the temperature is already above 0 °C and therefore no icing is predicted. Only at the beginning of this icing event, around 0200 UTC on 4 Jan 2017, when the temperature is very close to zero the model predicts icing, but due to the temperature very close to zero, the rather high LWC for cloud droplets and the high wind speeds, the accretion efficiency is very small for positions located close to the tip.

**Case 2: 8 Nov 2016 - 10 Nov 2016**

In the second case the camera images imply an ice load greater than light-moderate at the nacelle, while the SCADA data do not show icing at all. In figure 27, it is shown that, between 0600 UTC and 1300 UTC on 8 Nov 2016 the eologix sensors measured icing along the leading edge, except for the winglet and two sensors very close to the root, but the SCADA data did not register any icing. By looking at the power curve, one can see that the power decreases constantly during this icing event, even though the wind speed decreases slightly as well. Although, there is a decrease in the power probably partly due to icing, the algorithm in the SCADA data do not decide for icing. This might be caused by the rather low wind speed, which does not produce a lot of power at all.
This effect can also be observed for the icing event starting at 0000 UTC 9 Nov 2016, where again all sensors imply icing but there is no SCADA icing. Unfortunately, during the period of icing the eologix sensors and the wind turbine had an outage, so the wind turbine was shut down not necessarily due to icing, but because of technical problems. After the outage the eologix sensors closer to the tip did not show a significant icing anymore. This could be caused by ice throw or any ablation process, because the temperature was very close to 0 °C. Nevertheless, the camera images and also the sensors closer to the root still implied icing.
Schneider (2017) wrote that between 1200 UTC 9 Nov and 0600 UTC 10 Nov a rather significant rain event could be observed. This could mean that under freezing rain conditions bigger surfaces of attack are more prone to accrete ice than smaller ones. This would correspond with the basic equation 1, ignoring the impact of the efficiencies. Nonetheless, the SCADA data do not show any reaction to the icing close to the root. There are two possible ways to explain, why the power curve does not change. Firstly, as in case 1, due to the temperature close to 0 °C the ice type is glaze and therefore the aerodynamic effects are small and the wind turbine is not affected significantly. Another possible explanation could be that icing closer to the root has less impact on the aerodynamics than icing closer to the tip.

For this case study, since there is no blade heating, the eologix sensors and the ice rate based on the camera images show quite similar results, regarding the timing of the icing event. Especially for the first event they look nearly the same. But after the outage, only the sensors close to the root still notice icing, meaning that in this case there is a difference between the nacelle and the tip of the blade.

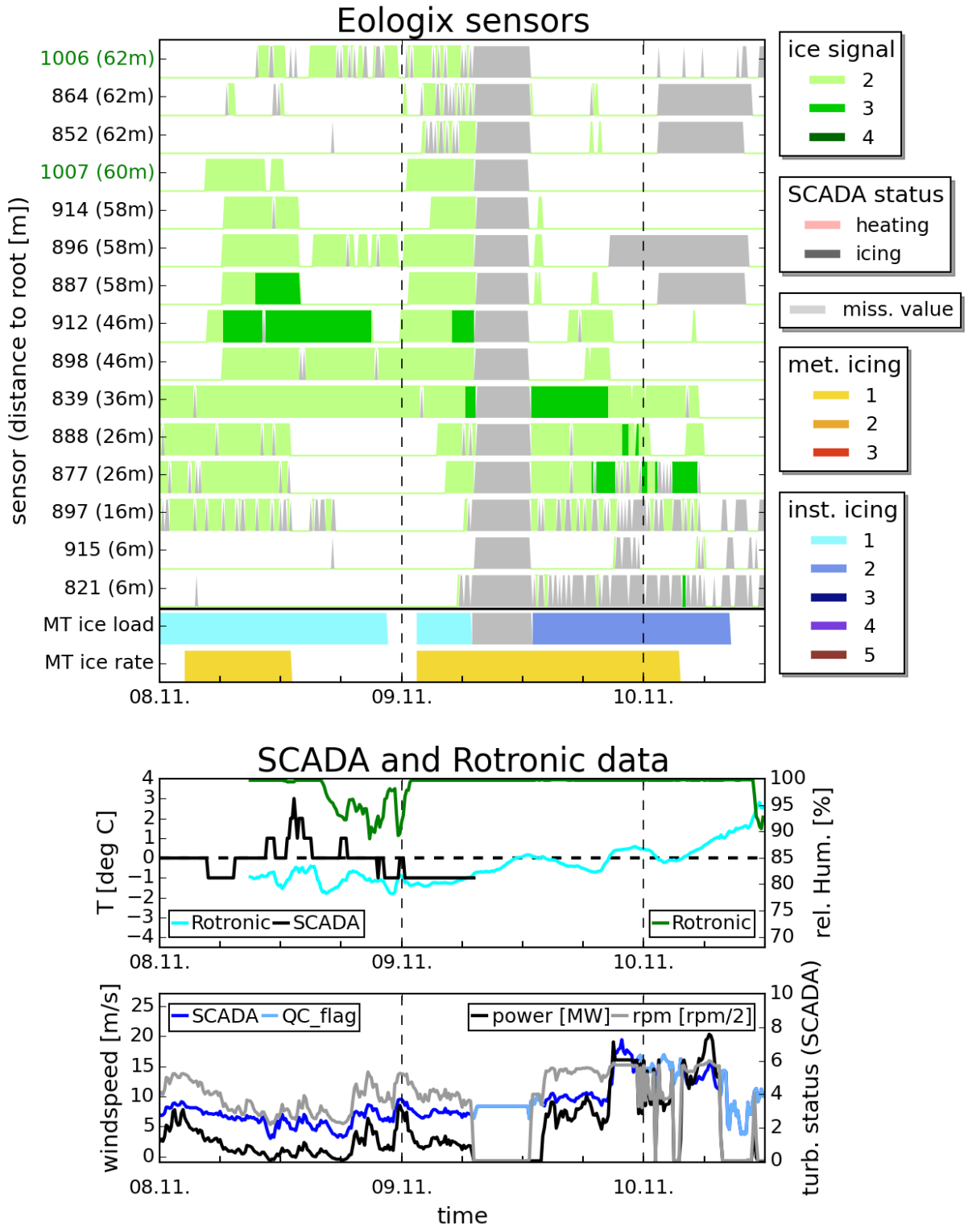


*Figure 27: iceBlade CASE 2: Overview of the observations made in the ICE CONTROL project for a wind turbine at Ellern from 0000 UTC 8 Nov 2016 to 1200 UTC 10 Nov 2016. Details are explained in section 6.*

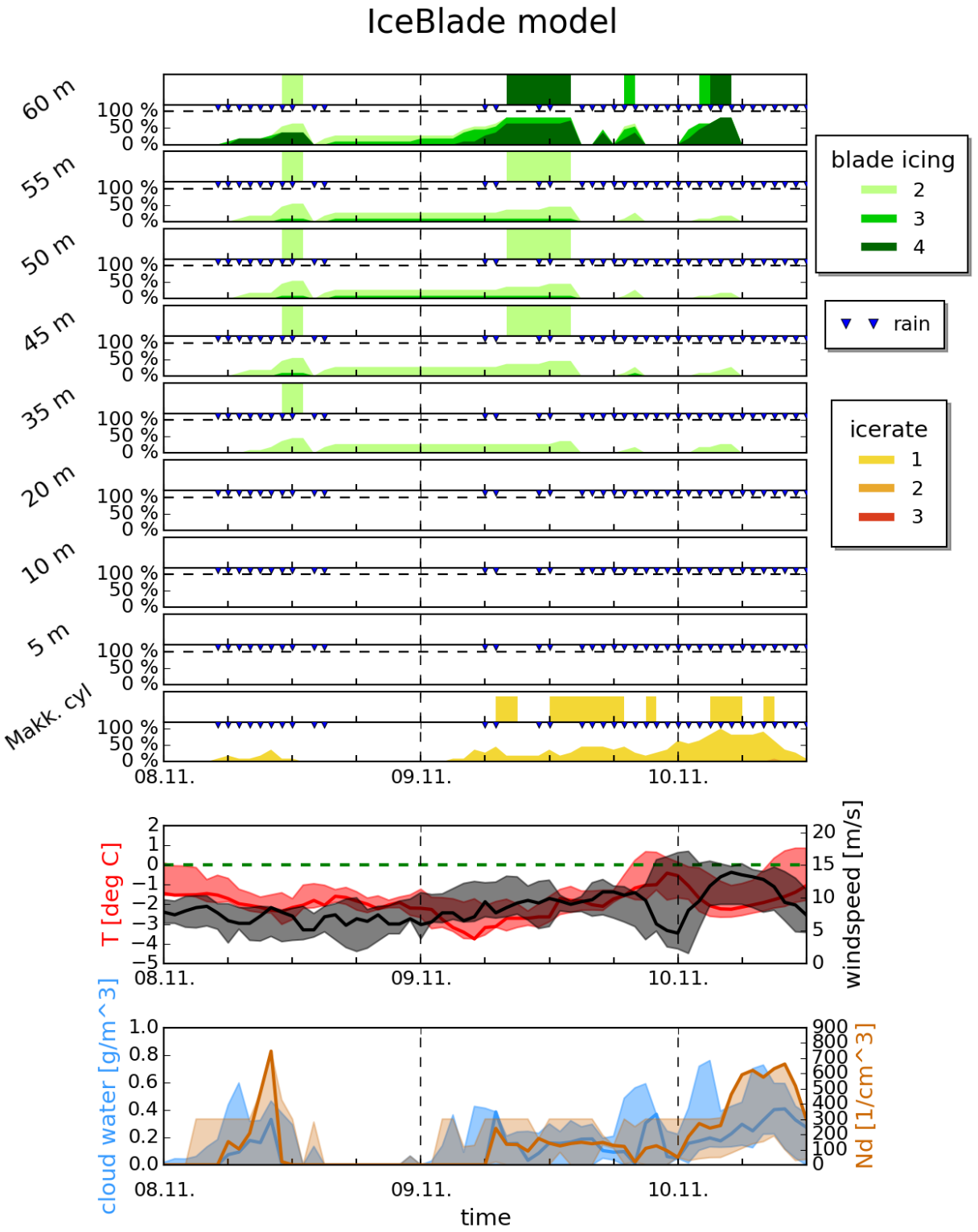


*Figure 28: iceBlade CASE 2: Icing prediction made by the iceBlade model for a wind turbine blade using an ensemble approach from 0000 UTC 8 Nov 2016 to 1200 UTC 10 Nov 2016. For each member of the WRFMP, 500 internal perturbed runs are computed. For comparison, the ice rate based on the Makkonen model is included. Details are explained in section 6.*

The results received with the iceBlade model again look rather similar to the observations from the eologix sensors, regarding the timing of the events. Especially the first short icing event on 1200 UTC 8 Nov correlates well with the observations. However, the distribution along the blade is not the same. While in the observations the icing event between 9 Nov and 10 Nov only effects the sensors closer to the root, the model predicts the icing again for outer positions. This time, only the first line is influenced by in-cloud icing, while the rest depends on icing due to rain drops.

Again, there is also a big uncertainty regarding the timing and the amplitude of the meteorological input parameters, especially the temperature and the wind speed at the end of the period. These uncertainties lead to errors, for example in the reference Makkonen model, which predicts the highest probability for a light icing rate at the end of the period, where the observations already imply positive temperatures. Also, for the first icing event, only a few members of the ensemble predict icing, using the Makkonen model.

Using these case studies some general results can be obtained.

The aim of these case studies is to determine, whether it is sufficient to use a reference cylinder rod as a proxy, which is located at the wind turbine's nacelle, to represent a wind turbine blade. By comparing these two cases, it is hard to give a general answer, because the Makkonen and the iceBlade model do not consistently agree or disagree with each other. Another difficulty is that even the observations have distinctions due to the rotation of the blade. There might be ablation processes, such as ice throw or also blade heating, which would not appear at the nacelle. This would be hard to be considered inside the Makkonen model. Moreover, using the Makkonen model makes it impossible to account for the ice distribution along the blade. Therefore, the iceBlade model is recommended, because in the end the aim is not to model icing in general, but to model icing that has an impact on the power of the wind turbine blade or on the safety of people.
In order to achieve the necessary quality, two improvements are needed. The first is an enhancement in predicting the correct meteorological input parameters to the icing models. In these case studies, one could see that although an ensemble is used, having different input and internal perturbed parameters, there are situations, in which icing is predicted wrongly. The other crucial key is to improve the representation of the turbine blade. The linear increase of the diameter towards the tip of the blade is too rough to make accurate predictions. Using a better blade representation would probably decrease the representative cylinder diameter and as a consequence the modelled distribution of the ice load would fit the observations better.

# 7 Conclusion

The aim of this thesis is to analyse empirical icing models and to identify their key uncertainties. To this end, two similar models, the Makkonen and the iceBlade model, are introduced. Based on the results of Weissinger (2017), the focus is mainly on in-cloud icing, but the prediction of icing due to freezing rain is also a part of these models. Icing events based on wet snow are not taken into account, since the simplifications necessary to predict these situations are too coarse.
Using the Makkonen model, the question of the most important uncertainties in the input parameters, received from a NWPmodel, is determined by varying them inside their typical range. Temperature, wind speed, LWC and droplet concentration are identified to produce the biggest uncertainties inside the icing model, in which LWC and droplet concentration cause additional uncertainties due to the lack of quantitative measurement methods.
By using normally distributed perturbations between +/- 10% of the original parameter values, the internal parameters, which are related to the uncertainty due to the imperfect representation of the physics inside the model, are varied. Their sensitivities are tested under different meteorological conditions. The ensemble range of the resulting ice loads is used to decide, to which parameter the model is the most sensitive. As a result, internal perturbations on the parameters related to the MVD seem to have the biggest impact in the icing models, although there is an uncertainty regarding parameters whose influence increases with increasing severity of the icing event. At the wind farm in Ellern during the winter in 2016/17, the icing events were rather weak and therefore these internal parameters have a smaller impact.
Comparing the importance of the input parameters to the internal parameters yields the result that it is crucial to predict the input parameters as accurately as possible. The internal parameters strongly depend on the input parameters. Therefore the question, if the input or the internal parameters are more important, is answered in favour of the input parameters. Even though under certain conditions, when the spread in the input parameter ensemble is small, the uncertainties in the internal parameters gain importance. Internal parameters related to the collision efficiency show a significant importance under the $\alpha_1$ regime (low LWC, low wind speeds and very low temperatures). Under the $\alpha_3$ regime (high LWC, high wind speeds and temperatures close to 0 °C) the models are very sensitive to internal parameters related to the accretion efficiency.
Instead of forecasting the ice load on a small cylindrical rod, the iceBlade model is used to predict icing on a wind turbine blade. Having higher velocities due to the additional rotation and bigger cylinder diameters, some additional simplifications were made. Adaptations regarding the empirical fit for the collision efficiency were added, even though the accuracy of this fit still suffers from the bigger cylinder diameter and the higher wind speeds. Using the iceBlade model, the validity of taking a simplified small cylinder as a proxy for wind turbine blades is tested under real conditions. Due to the lack of the spatial distribution of the ice load along the blade in the Makkonen model, the use of the iceBlade model is recommended. The discrepancies between the measurement instruments at the nacelle and on the blade support the theory that it is important to predict the ice load directly on the wind turbine blade. Nonetheless a general result, answering the question, if the Makkonen model prediction is enough to model icing on a blade cannot be found. The reason is that there is no consistent correlation between the Makkonen and the iceBlade model. This is probably partly caused by the rough geometric representation of the blade, leading to errors in the resulting ice loads for the iceBlade model.

## 7.1 Outlook

Future works can try to improve modelling the blade more realistically to achieve a better distribution of the ice load along the blade for the iceBlade model.
Another important point is to expand the empirical fit for the collision efficiency to situations typical for wind turbine blades. The best way would be to run simulations using advanced icing models to predict the trajectories of the droplets and to make wind tunnel experiments to verify them and to establish an empirical fit for the collision efficiencies for turbine blades. Unfortunately, this is rather expensive.
To get a better understanding of the model, it is important to have a good comparison to verify the results. The eologix sensors, used in this thesis, showed some promising results, but it would be necessary to distinguish between rime and glaze ice, since they have different aerodynamic characteristics. Maybe this could be accomplished by using camera images directed towards the wind turbine blade. In this thesis, the most sensitive internal parameters are selected, but a quantitative verification could not be done due to the small amount of icing data available. In the course of the ICE CONTROL project, additional wind turbine farms will be used, as marked in figure 13. Having these data sets, it will be possible to do an ensemble verification in order to determine the value of perturbing the most important internal parameters.
These ideas are just a few of many possibilities to improve the prediction of icing for wind turbines. Not only ice accretion, but also ice ablation processes, such as evaporation or ice shedding, still cause a lot of problems and can be treated in the future projects.

# Bibliography

Andersen, E., E. Börjesson, P. Vainionpää, and L. S. Undem, 2011: REPORT - Wind Power in cold climate. Tech. rep., WSP Environment & Energy Sweden.

Bergmann, and Schaefer, 2001: *Lehrbuch der Experimentalphysik - Erde und Planeten*. 2nd ed., 191 pp.

Burchhart, T., 2017: ICE - CONTROL: Eologix Vereisungsdetektion. presentation. VERBUND.

Burchhart, T., 2018: ICE - CONTROL: Innovative icing measurements and icing forecasts to optimize the operation of wind farms during icing conditions. URL windren.se/WW2018/09_3_11_Burchhart_ICE_CONTROL_Potential_of_innovative_icing_measurements_and_icing_forecasts_to_optim pdf, presentation. VERBUND.

Cattin, R., and U. Heikkilä, 2016: Evaluation of ice detection systems for wind turbines. Tech. rep., Meteotest.

Davis, N., A. N. Hahmann, and N.-E. Clausen, 2014: Forecast of icing events at a wind farm in sweden. *Journal of applied Meteorology and Climatology*, **53**, 262–281, doi:10.1175/JAMC-D-13-09.1.

Davis, N. N., 2014: Icing Impacts on Wind Energy Production. phdthesis, Technical University of Denmark.

Elíasson, A. J., H. Ágústsson, G. M. Hannesson, and E. Thorsteins, 2014: Modelling wet-snow accretion - Comparison of cylindrical model to field measurements.

Errico, R. M., 1997: What is an adjoint model. *Bulletin of the American Meteorological Society*, 2577–2591, doi:10.1175/1520-0477(1997)078<2577:WIAAM>2.0.CO;2.

Finstad, K. J., E. P. Lozowski, and E. M. Gates, 1987: A computional investigation of water droplet trajectories. *Journal of Atmospheric and Oceanic Technology*, **5**, 160–170, doi:10.1175/1520-0426(1988)005<0160:ACIOWD>2.0.CO;2.

Finstad, K. J., E. P. Lozowski, and L. Makkonen, 1988: On the median volume diameter approximation for droplet collision efficiency. *Journal of the Atmospheric Sciences*, **45**, 4008–4012, doi:10.1175/1520-0469(1988)045<4008:OTMVDA>2.0.CO;2.

Homola, M. C., T. Wallenius, L. Makkonen, P. J. Nicklasson, and P. A. Sundsbø, 2010: Turbine size and temperature dependence of icing on wind turbine blades. **34**, 615–628.

IMGW, 2017: ICE CONTROL: Verbesserung der Prognose von Vereisung an Windkraftanlagen. URL https://imgw.univie.ac.at/research/general-meteorology-and-climatology/projects/ice-control/.

ISO 12494, 2012: Atmospheric icing of structures. Tech. rep., International Organization of Standardization.

Jonkman, J., S. Butterfield, W. Musial, and G.Scott, 2009: Definition of a 5-MW Reference Wind Turbine for Offshore System Development. Tech. rep., National Renewable Energy Laboratory.

Kochtubajda, B., and E. Lozowski, 1985: The Sublimation of Dry Ice Pellets Used for Cloud Seeding. *Journal of Climate and applied Meteorology*, **22**, 597–605.

Krambeck, D., 2015: An introduction to scada systems. URL https://www.allaboutcircuits.com/technical-articles/an-introduction-to-scada-systems/.

Laakso, T., and Coauthors, 2010: State-of-the-art wind energy in cold climates. resreport, VTT Technical Research Centre of Finland.

Langmuir, I., and K. Blodgett, 1946: A mathematical investigation of water droplet trajectories. *Collected works of Irving Langmuir*, **10**, 335–393.

Lehtomäki, V., and Coauthors, 2016: IEA Wind Task 19: Available Technologies of Wind Energy in Cold Climates. resreport, VTT Technical Research Centre on Finland Ltd.

Ludlam, F., 1951: The heat economy of a rimed cylinder. *Royal Meteorological Society*, **77**, 663–666, doi:10.1002/qj.49707733410.

Macklin, W. C., 1962: The density and structure of ice formed by accretion. *Royal Meteorological Society*.

Makkonen, L., 1984: Modeling of Ice Accretion on Wires. *Journal of Climate and applied Meteorology*, **23**, 929–939, doi:10.1175/1520-0450(1984)023<0929:MOIAOW>2.0.CO;2.

Makkonen, L., 2000: Models for the growth of rime, glaze, icicles and wet snow on structures. *Phil. Trans. R. Soc.*, **358 A**, 2913–2939, doi:10.1098/rsta.2000.0690.

Makkonen, L., and J. Stallabrass, 1984: Ice accretion on cylinders and wires. Tech. rep., National Research Council of Canada.

Makkonen, L., and J. Stallabrass, 1987: Experiments on the cloud droplet collision efficiency of cylinders. *Journal of Climate and applied Meteorology*, **26**, 1406–1411, doi:10.1175/1520-0450(1987)026<1406:EOTCDC>2.0.CO;2.

Mazin, I., A. Korolev, A. Heymsfield, G. Isaac, and G.Cober, 2001: Thermodynamics of icing cylinder for measurements of liquid water content in supercooled clouds. *Journal of Atmospheric and Oceanic Technology*, **18**, 543–558.

Molinder, J., 2018: Addressing forecast uncertainty of wind turbine icing with deterministic sampling. presentation. Uppsala Universitet.

Pedersen, M. C., H. Sorensen, N. Swytink-Binnema, B. Martinez, and T. Condra, 2018: Measurements from a cold climate site in Canada: Boundary conditions and verification methods for CFD icing models for wind turbines. *Cold Regions Science and Technology*, **147**, 11–21, doi:10.1016/j.coldregions.2017.12.007.

Ronsten, G., 2008: Mapping of Icing for Wind Turbine Applications - A Feasibility Study. Tech. rep., Elforsk.

Schneider, M., 2017: Case studies of wind turbine icing at a wind farm in Ellern, Germany, during winter 2016/17.

Söderman, J. P., H. Körnich, E. Olsson, H. Bergström, and A. Sjöblom, 2017: Probabilistic forcasting of wind power production losses in cold climates: A case study. *Wind Energ. Sci. Discuss.*, doi:10.5194/wes-2017-28.

Strauss, L., and S. Serafin, 2018: ICE CONTROL meeting 20180316. presentation.

Thompson, G., and T. Eidhammer, 2014: A Study of Aerosol Impacts on Clouds and Precipitation Development in a Large Winter Cyclone. *Journal of the Atmospheric Sciences*, **71**, 3636–3658, doi: 10.1175/JAS-D-13-0305.1.

Thompson, G., B. E. Nygaard, L. Makkonen, and S. Dierer, 2009: Using the weather research and forforecast (wrf) model to predict ground/structural icing.

Thompson, G., M. K. Politovich, and R. M. Rasmussen, 2017: A Numerical Weather Model's Ability to Predict Characteristics of Aircraft Icing Enviroments. *Weather and Forecasting*, **32**, 207–221, doi: 10.1175/WAF-D-16-0125.1.

Turkia, V., S. Huttunen, and T. Wallenius, 2013: Method for estimating wind turbine production losses due to icing. resreport, VTT Technical Research Centre of Finland.

United Nations, 2015: Paris Agreement. URL https://unfccc.int/sites/default/files/english_paris_agreement.pdf.

VERBUND, 2016: Drahtlose Eisdetektion und Temperaturmessung. presentation.

Weissinger, M., 2017: Synoptische Analyse von Vereisungsfällen an Windkraftanlagen am Beispiel Ellern, Deutschland.

Winter WX, n.d.: Freezing Rain. URL https://www.weather.gov/source/zhu/ZHU_Training_Page/winter_stuff/winter_wx/winter_wx.html.

WIREs Energy Environ, 2016: **5**, 128–135, doi:10.1002/wene.170.

World Energy Council, 2016: World Energy Scenarios. resreport.

# List of Tables

# List of Figures